INVESTIGATIONS ON THE UNCERTAINTIES IN PLUTONIUM TO CURIUM-244 RATIO METHOD OF PLUTONIUM ACCOUNTANCY IN PYROPROCESSING

A Thesis

by

HEUKJIN BOO

Submitted to the Office of Graduate and Professional Studies of
Texas A&M University
in partial fulfillment of the requirements for the degree of

MASTER OF SCIENCE

Chair of Committee,	Sunil S. Chirayath
Committee Members,	Jonathan Burns
	Matthew Fuhrmann
Head of Department,	John E. Hurtado

August 2019

Major Subject: Nuclear Engineering

ABSTRACT

The objective of this project study is to analyze the non-uniformity of used fuel assembly nuclide compositions and to estimate the effect of this non-uniformity in Pu accountancy using the Pu-to-^{244}Cm ratio method for pyroprocess. In order to estimate the nuclide compositions as a function of axial and radial location in used fuel, simulation of fuel burnup is performed using Monte Carlo N-Particle 6 (MCNP6) code. The simulation model used is a one-eighth model of a 17x17 fuel assembly which is divided into 9 axial and 2 radial meshes for each fuel rod.

The axial and radial non-uniformities of nuclide compositions of used fuel obtained from the MCNP6 code burnup simulation are analyzed. The axial neutron flux distribution is found to play an important role in the axial non-uniformity of nuclide compositions. In addition, the rim (edge) effect causes the radial distribution of the non-uniformity. Therefore, the Pu-to-^{244}Cm ratio varied in the fuel depending on the location. Hence, the Pu-to-^{244}Cm ratio method used in plutonium accounting will get affected. Depending on where the samples are chosen from the chopped pieces in estimating the Pu-to-^{244}Cm ratio at the head-end of the pyroprocess, the uncertainties due to non-uniformity can negatively impact the accuracy of the plutonium accounting method. However, if the used fuel powders from the voloxidation step in pyroprocess are used as samples for the Pu-to-^{244}Cm ratio method, the uncertainties are found to be small. In addition to estimating plutonium accounting uncertainty due to the used fuel nuclide composition non-uniformity, error propagation through the key-pyroprocesses (the electrolytic reduction, the electrorefining, and the electrowinning) are performed to calculate the Material Unaccounted For (MUF) in the assumed Material Balance Area (MBA) for the pyroprocessing facility. The available throughput to fulfill the IAEA (International Atomic Energy Agency) nuclear material safeguards criteria is also estimated for a given Material Balance Period (MBP).

Based on the observations, although the variance of nuclide compositions exists in used fuel, it can be concluded that the non-uniformity of nuclide compositions in a used fuel does not influence the Pu material accountability using the Pu-to-^{244}Cm ratio method in pyroprocessing when samples are taken from the voloxidation step of the pyroprocess.

DEDICATION

First of all, I want to mostly dedicate this study to my precious wife, Arikoen Sung, who has spent most of her time in the United States for supporting my study and taking care of our lovely daughter, Yesol Boo. Also, this work is dedicated to my country and the Republic of Korea Army that have been funding my living and study in the United States for two years.

ACKNOWLEDGEMENTS

I want to thank my committee chair, Dr. Chirayath, and my committee members, Dr. Burns, and Dr. Fuhrmann, for their guidance and support for this research.

In addition, thanks to all of my friends in Jeju and Yu-shin 6th Company friends who have been always willing to cheer me, especially Heejong, Junbeom, Minwoo, Minjeong, Mijin, Soohoon, Daesung, Yunchang, Seungsuk, Chiun, Seunghoon, Junghwan, Jungsuk, Hoonsuk, Namjin, Yunho, and Heehyun. Also, my sincerest apologies for not attending wedding ceremonies of Seungsuk, Minjeong, and Mijin because of the Army's regulation which prohibits returning to South Korea before obtaining a degree.

Thanks also go to Dr. Seungmin Woo and Dr. Changwoo Kang who gave me motivation and a good idea for this study. Especially, Dr. Woo spent a lot of time to support this project despite of his busy schedule.

Moreover, I am very grateful to Seungmin, Jinsu, Sungkyu, Byungkyu, Yeongchan, Junseob, and Duhwan who are Korea Military Academy alumnus studying in College Station and have been the pride of the ROK Army.

Finally, thanks to my family in South Korea, Namjoon Boo, Yeongsook Yoo, Hyeonho Sung, Yongyoung Kim, Kukjin Boo, Soyeon Park, Sodam Sung, Jedo Lee, and Seojoon Lee for their understanding and encouragement.

CONTRIBUTORS AND FUNDING SOURCES

Contributors

This work was supervised by a thesis committee consisting of Dr. Chirayath as a committee chair and Dr. Burns of the Department of Nuclear Engineering and Dr. Fuhrmann of the Department of Political Science.

The overall approach for this study was inspired by the dissertation of Dr. Woo. The fuel assembly burnup simulation using MCNP6 for Chapter 3 was helped by Dr. Woo. The development of the sampling method using MATLAB code to investigate the effect of the non-uniformity of nuclide compositions was also advised by Dr. Woo. The powder size distribution data for Chapter 2 was referred from the paper, sintering of mixed UO_2 and U_3O_8 powder compacts, published by Dr. Kunwoo Song.

All other work conducted for the thesis was completed by the student independently.

Funding sources

This graduate study was funded by a fellowship from the Republic of Korea Army Headquarter scholarship program.

NOMENCLATURE

IAEA	International Atomic Energy Agency
NDA	Non-Destructive Analysis
DA	Destructive Analysis
MCNP	Monte Carlo N-Particle code
MUF	Material Unaccounted For
MBA	Material Balance Area
MBP	Material Balance Period
KMP	Key Measurement Point
NMA	Nuclear Material Accountancy
KAERI	Korea Atomic Energy Research Institute
TRU	Transuranic
ITV	International Target Value
IDMS	Isotope Dilution Mass Spectrometry
HLNC	High Level Neutron Coincidence Counter
SF	Spontaneous Fission

TABLE OF CONTENTS

Page

LIST OF FIGURES

Page

Page

LIST OF TABLES

Page

CHAPTER I

INTRODUCTION

Background

Pyroprocessing of used nuclear fuel has been extensively studied by Korea Atomic Energy Research Institute (KAERI) for recycling used fuels in a closed nuclear fuel cycle[1]. KAERI is interested in this process because pyroprocessing technology has many advantages: (1) greater radiation-resistance to the process fluids, (2) final nuclear waste reduction, and (3) the possibility of compact facility design when compared to wet used fuel reprocessing such as that of PUREX process[2].

Pyroprocessing consists of the head-end process (mainly chopping and voloxidation), electrolytic reduction, electrorefining process, electrowinning system, and waste treatment process[1]. The feed materials that are used nuclear fuel assemblies are processed in the head-end process by each fuel rod getting axially chopped. Then, the chopped pieces undergo voloxidation process where uranium dioxide (UO_2) is the solid form is oxidized to U_3O_8 in a powder form to make its surface area larger[2]. After the voloxidation process, the feed powder material is transferred to the electroreduction process, which is the first process of the key-pyroprocess in order to reduce the fuel powders into a metallic form. In this electrolytic reduction process, actinides in oxide form are reduced to metallic form (M) as shown in Eq. 1[2].

$$M_xO_y + 2yLi \rightarrow xM + yLi_2O \qquad \text{Eq. 1}$$

As this process progresses, most alkaline (A) and alkaline earth (AE) metals are transformed to dissolved metal chlorides in the molten salt and, eventually, removed as wastes. For rare earth (RE) elements, the unreduced REs in oxide form are contained in the dross floating above the

molten metal. The dross is also eliminated from the molten metal as wastes[2]. A portion of the RE, however, is not reduced because of the reduction rate depending on the concentration of Li_2O in the molten salt[2]. As a result of this process, most uranium (U), transuranic (TRU) elements, and some RE elements, which are then transferred to the electrorefining process as feed material are obtained from the salt by filtering[2]. After the electrolytic reduction process, the electrorefining is processed to recover U from the feed materials from the previous process. The feed material is collected at the anode except U and TRU, which is enclosed by LiCl-KCl solution. More specifically, the following reactions, $U \rightarrow U^{3+} + e^{3-}$ at the anode and $U^{3+} + e^{3-} \rightarrow U$ helps to deposit U onto the cathode. By using this, the U product in the U-ingot form is obtained at the cathode and please note that this is depleted U. On the other hand, TRU, RE, and a small amount of U are still remaining in the molten salt. These remaining metals then go to the next process, the electrowinning process to store TRU and the small amount of U on to a second cathode, which is possible by adjusting the electrochemical potential supplied to the molten salt. In this process, all TRUs and the remaining U are obtained in the liquid cadmium cathode (LCC)[1].

As described above, in a pyroprocessing facility, depleted U ingots and U-TRU ingots are produced by processing used nuclear fuel. U-TRU ingots contain TRU elements such as neptunium (Np), Pu, americium (Am), Cm mixed with depleted uranium nearly in the ratio U:TRU as 1:1. In addition to its composition, the geometry of U-TRU ingot has not been decided, but the size of U-TRU ingot is assumed to be 4 cm (D) × 4.2 cm (H), 1 kg of mass, and 19 g/cm^3 of mass density in the reference literature[3]. In this study, Pu and ^{244}Cm mass densities are considered so the volume of U-TRU ingot is not used. Since Pu material accountancy in U-TRU product ingot is very important with respect to the proliferation risk, Nuclear Material Accountancy (NMA) methods should be established before operating a pyroprocessing facility. One of the performance metrics

to evaluate NMA methods is the estimation of Material Unaccounted For (MUF), which is defined as the difference between the book inventory, the algebraic sum of the most recent physical inventory in a Material Balance Area (MBA) and of all the inventory changes that have occurred since that physical inventory. The physical inventory is the sum of all the measured or derived estimates of batch quantities of nuclear material on hand at a given time within a MBA[4] and, therefore, the MUF should be accurately evaluated for each MBA.

The Pu-to-^{244}Cm ratio method had been developed to measure Pu content so it can be utilized for the NMA in the reprocessing system including pyroprocessing[5]. For this method, the representative Pu-to-^{244}Cm ratio of a used nuclear fuel assembly should be accurately evaluated at the beginning of the pyroprocess (at the fuel rod chopping step). In addition, it is important that a neutron detector is properly used as a Non-Destructive Assay (NDA) method to measure the mass of ^{244}Cm since most neutrons emitted from the used fuel are produced by the Spontaneous Fission (SF) of ^{244}Cm, which can be done during the process including the product (U-TRU ingot) retrieval step. By multiplying two measured data, the Pu-to-^{244}Cm ratio (at the pyroprocess beginning) and the ^{244}Cm mass (measured at the end of the pyroprocess), the mass of Pu can be indirectly measured as shown in Eq. 2. By comparing the Pu content calculated in the head-end process to the Pu amount during the process measured by the Pu-to-^{244}Cm ratio method, the MUF for the defined MBA and the Material Balance Period (MBP) can be practically measured.

$$\mathrm{Pu} = \left(\frac{\mathrm{Pu}}{^{244}\mathrm{Cm}} \right)_{\mathrm{HeadendProcess}} \times {}^{244}\mathrm{Cm}_{\mathrm{Any\ step\ of\ Pyroprocessing}} \qquad \text{Eq. 2}$$

Since Pu and ^{244}Cm nuclide compositions is not uniform depending on the location in the used nuclear fuel assembly and hence the Pu-to-^{244}Cm ratio value can influence the Pu accountancy method. In this study, this non-uniformity of Pu and Cm compositions are considered as a source of uncertainty in Pu NMA in the pyroprocessing system. Fuel burnup simulations to obtain the

non-uniform composition data in the used fuel assembly is conducted as a first step using the radiation transport code, MCNP6 embedded in which is the fuel burnup code CINDER90[6]. The location-dependent nuclide composition data thus obtained for used nuclear fuel (the feed material in pyroprocess) is utilized as the primary input for the studying the effect on the accuracy of Pu accountancy using the Pu-to-^{244}Cm ratio method. Design parameters of a nuclear fuel assembly for the depletion calculation are based on the nuclear fuel assembly of Westinghouse design[7]. Then, in order to estimate the uncertainties of the Pu-to-^{244}Cm ratio from the chopping process (case-1) and the voloxidation process (case-2), nuclide compositions of each fuel rod in the depleted fuel assembly are appropriately modified. The sampling of nuclear material to estimate the Pu-to-^{244}Cm ratio in the head-end process is performed using MATLAB code. Also, the NDA equipment (coincidence neutron detection system) model using MCNP6 is utilized to estimate the ^{244}Cm mass during the process for the Pu material accountancy. Finally, the MUF and the standard deviation of the MUF for two cases, taking samples after the i) chopping and ii) voloxidation processes, are calculated to evaluate NMA in a pyroprocessing facility by comparing those values with 8 kg of Pu which is the Significant Quantity (SQ) defined as the approximate amount of nuclear material that cannot be excluded from the possibility of producing a nuclear explosive device[8].

Previous Work

There were previous studies with respect to the nuclear material safeguards for a pyroprocessing facility. Kim studied the development of the design information and nuclear material safeguards approach for the reference engineering scale pyroprocess facility to enhance safeguards[9]. Moreover, available approaches to evaluate the Pu mass of used nuclear fuel

assemblies in pyroprocess using NDA and burnup simulation code are reported by Lee et al[10]. In addition, a hybrid concept of Pu accountancy in the U-TRU ingot is proposed by Seo et al[3]. There was also research investigation on a potential nuclear material diversion from a pyroprocessing facility which is conducted by Woo et al[11]. However, those studies do not include investigations on the effect of non-uniformity of nuclear composition in used nuclear fuel in a pyroprocessing system until Woo[12] proposed it in 2018.

In Woo's research, the same particle size was assumed in estimating the uncertainty of the Pu-to-^{244}Cm ratio for the voloxidation process. In order to develop more reliable sampling schemes in this study, the method reflecting the variation of powder sizes that can be obtained from the reference[13] is developed. Moreover, the performance metric of his previous study was the Type-I error calculated by the hypothesis testing method. The criterion of that study is the Type-I error should be less than or equal to 5%. On the other hand, in this study, the MUF and the sigma MUF estimated are compared to the SQ value to ensure that the NMA of the facility meets the IAEA's criteria.

Furthermore, the mesh configuration for the fuel burnup simulation of the nuclear fuel assembly in this study differs from that in Woo's study. The criteria of designing meshes in this project are based on a comparison between MCNP's stochastic uncertainties of ^{238}U neutron capture reaction rate, which is a dominant path of producing ^{239}Pu and the non-uniformity of Pu defined as the difference of Pu between each spatial location in used nuclear fuel. More specifically, meshes are designed to have the stochastic uncertainty to be less than the calculated non-uniformity of Pu. This is because if the stochastic uncertainty is greater than the non-uniformity of Pu in an established mesh it cannot be considered that each mesh shows the real non-uniformity in Pu. Initially, each fuel rod was divided into 13 axial meshes and 3 radial meshes.

However, some of the meshes are combined until their stochastic simulation uncertainties are smaller than their Pu non-uniformity. As a consequence of these criteria, the fuel rod is divided into 9 axial and 2 radial meshes for the MCNP6 modeling and simulations. Therefore, the mesh configuration of fuel rods is different from that in Woo's research[12].

Objective

The objective of this project study is to analyze the non-uniformity of used fuel assembly nuclide compositions and to estimate the effect of this non-uniformity in Pu accountancy using the Pu-to-^{244}Cm ratio[5] method for pyroprocess. The Pu-to-^{244}Cm ratio method is based on the fact that Cm is dominant neutron source in a used fuel assembly[5,10]. If the Pu-to-^{244}Cm ratio in a used nuclear fuel can be measured before the used fuel assembly is processed in a pyroprocessing facility, the Pu mass during the process can be measured by multiplying the measured Pu-to-^{244}Cm ratio at the head-end process by the ^{244}Cm mass obtained at any step of pyroprocessing using neutron coincidence counting. However, if there are non-uniformities Pu and Cm composition in a used fuel assembly due to spatial location, it could affect the evaluation of the Pu-to-^{244}Cm ratio and hence the Pu accountancy. The objective of this study is also to investigate the effect of such a non-uniformity in a used fuel on Pu accountancy in pyroprocessing and to optimize the nuclear material safeguards approach for this process.

CHAPTER II

METHODOLOGY

Overall Approach

In order to investigate the uncertainties in the Pu-to-^{244}Cm ratio method in pyroprocessing NMA, the fuel burnup calculation is simulated using MCNP6 code to prepare the inputs for the studies. This simulation is conducted to obtain nuclide compositions in a used nuclear fuel assembly which is the feed material in pyroprocessing. The obtained nuclide compositions then should be examined to determine whether the stochastic uncertainty of MCNP6 code predictions is greater than the non-uniformity of Pu in an established mesh. This examination is required to make sure the actual non-uniformity in nuclide compositions is not as a result of stochastic uncertainty, an inherent feature of MCNP6 code. Therefore, MCNP6 code predicted stochastic uncertainties of the ^{238}U neutron capture reaction, which is a dominant path of producing ^{239}Pu, are compared to the non-uniformity of Pu, which is defined as the difference in Pu between each spatial location in used nuclear fuel pin. In other words, the MCNP6 code's predicted stochastic uncertainties should be verified to be less than the non-uniformity for each mesh for the input required for this study.

After the verification of the data from the depletion simulation, the Pu-to-^{244}Cm ratio uncertainty is evaluated by modeling and simulating the sampling of chopped fuel pieces after the chopping process of the head-end process using MATLAB code. Each fuel pin is axially divided in lengths of 1 cm and 0.8 cm. Because the radial non-uniformity of nuclide composition in a fuel rod is not important for this chopping process, the nuclide composition data in the radial meshes is shown as an average value of those radial meshes. For estimating Pu and ^{244}Cm contents, which

are required to obtain the Pu-to-^{244}Cm ratio using the Destructive Assay (DA) technique such as the K X ray fluorescence analysis[14], random sampling of chopped pieces is modeled. Then, the uncertainty of the Pu-to-^{244}Cm ratio is estimated by assuming that samples are taken after the chopping process.

Furthermore, in order to calculate the uncertainty in the voloxidation process, the type of U_3O_8 powder size distribution[13] is defined by hypothesis testing. The Pu-to-^{244}Cm ratio uncertainty of U_3O_8 powder samples, taken from the voloxidation process, in an assumed lab spoon (0.05 ml, 0.1 ml, and 0.5 ml) is then estimated using MATLAB code. Since the U_3O_8 powder sizes in the spoon are varied, the powder size distribution[13] is applied to model the sampling scheme. In the MATLAB simulation, sampling powder particles is continued unless the cumulative volume of sampled particles is the same as the volume of the assumed lab spoon. After iterating this sampling scheme, the average and standard deviation of the Pu-to-^{244}Cm ratio among those trials are computed.

Then the MUF and the standard deviation (one sigma) of the MUF for two cases which consist of taking samples after the chopping and the voloxidation processes are estimated. The MBA is also established and the sigma MUF is obtained for the established MBA, for instance considering the entire pyroprocess system, by propagating the uncertainties of detectors used and evaluating the Pu-to-^{244}Cm ratio value. As a result, the sigma MUF (standard deviation in MUF measurements) is compared to the criteria of IAEA for the NMA, which are a) the MUF should be less than 1 SQ, b) the MUF should be less than three times the standard deviation in the MUF measurements, and c) three times the standard deviation of the MUF should be less than 1 SQ.

Finally, the effect of the non-uniformity of nuclide compositions in used nuclear fuel in the estimation and accounting of Pu in pyroprocessing is analyzed. In addition, the NMA at a hypothetical pyroprocessing facility is discussed by analyzing the calculated results thus obtained.

Nuclear Fuel Assembly Depletion Calculation by MCNP6

In order to obtain the nuclide composition of the used nuclear fuel assembly, fuel burnup simulation is conducted using MCNP6 code[6]. The design parameters of a nuclear fuel assembly for the depletion simulation are based on the nuclear fuel assembly designed by Westinghouse (17×17)[7]. The radii of fuel pellet, an inner cladding, and outer cladding are 0.39, 0.40, and 0.46, respectively. There is a vacuum gap between the fuel and the cladding. The pitch of a fuel pin is 1.26 cm including the moderator which is water surrounding the fuel pin. The height of each fuel rod is 365.8 cm. This single fuel pin has 18 meshes, 9 axial and 2 radial meshes, as shown in Figure 1 and listed in Table 1. In a fuel assembly, the moderator density changes depending on the change of temperature in the axial direction. Therefore, the axial neutron flux distribution is influenced by this, so the 9 axial meshes are established to reflect this. The axial temperature distribution can be calculated using Eq. 3[15].

$$T_{H_2O}(z) = T_{in} + \frac{q_0^{'}\tilde{H}}{\pi C_p w}\left[\sin\left(\frac{\pi z}{\tilde{H}}\right) + \sin\left(\frac{\pi H}{2\tilde{H}}\right)\right] \qquad \text{Eq. 3}$$

Where,

$T_{H_2O}(z)$ = water temperature as a function of axial location z

T_{in} = inlet water temperature in the reactor

w = water flow rate

C_p = water heat capacity

H = fuel length

$\tilde{H}$ = extrapolation length

$$q_0^{'} = \pi r^2 w \sum_f \phi_0 J_0 \left(\frac{2.405 r_f}{\tilde{R}} \right)$$

The U enrichment of the entire fuel assembly is assumed as 3.3 at % of ^{235}U. Details of the design parameters of the fuel used in the MCNP6 model are listed in Table 2, 3, and 4. In order to minimize the leakage of neutrons in the axial direction, water reflectors of 50 cm thickness are placed at the top and bottom of the fuel assembly.

In order to reduce the calculation time, only one-eighth of one PWR nuclear fuel assembly as shown in Figure 2 is simulated since a fuel assembly has one-eight symmetry. The one-eighth fuel assembly includes 12 universe regions (MCNP6 code terminology) regions along the radial direction from the center to determine the non-uniformity in nuclide compositions. 12 different colors of the UO_2 fuel rod indicate their universe region number and is shown in Figure 3. This means the one-eighth assembly consists of 216 materials, which is calculated as 9 axial meshes multiplied by 2 radial meshes multiplied by 12 universes. A reflective boundary condition is assumed on all sides of the one-eighth fuel assembly except on top and bottom.

Operating conditions for this simulation are also referred from the Westinghouse Pressurized Water Reactor (PWR)[7]. Average power of one nuclear fuel assembly is 17.67 MWth which is computed by a total thermal power of the reactor core divided by the number of assemblies in the reactor core. Therefore, 2.20875 MWth, one-eighth of 17.67 MWth, is set for the one-eighth fuel assembly in the MCNP6 code fuel burnup simulation input. Because the temperature of the moderator is sensitive in the depletion simulation by MCNP6 code, the axial water temperature distribution is estimated by applying the energy conservation equation between the heat generation by the fuel assembly and the cooling properties of water[15]. 20,000 source

neutrons per criticality calculation cycle, 500 active neutron generation cycles, and 25 inactive cycles are used in this simulation. The MCNP6 code input deck used for this simulation is attached in Appendix A.

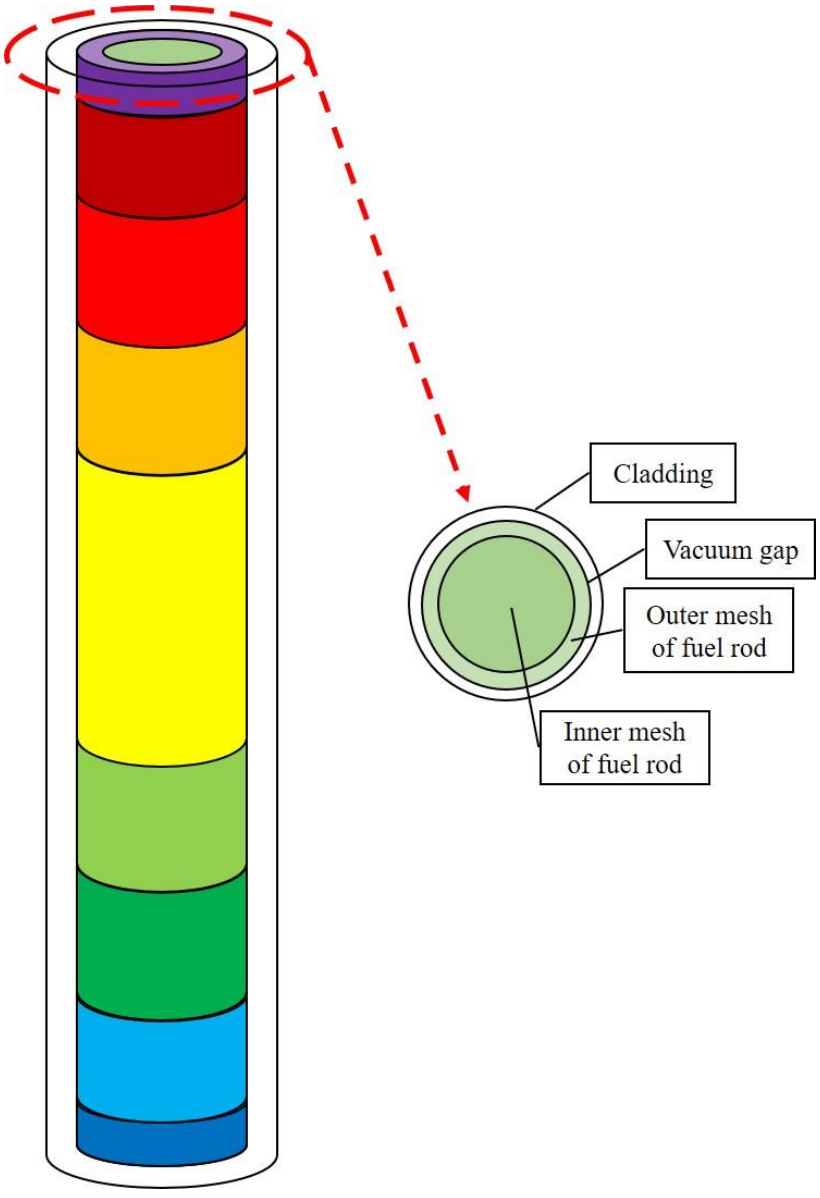

Figure 1. Design of the Simulated UO_2 Fuel Rod.

Table 1. Axial and Radial Mesh Configuration of the Single Fuel Pin.

Axial	
Mesh	Height [cm]
1st	2.779
2nd	8.251
3rd	13.474
4th	40.83
5th	235.132
6th	40.83
7th	13.474
8th	8.251
9th	2.779
Total	365.8
Radial	
Mesh	Radius [cm]
Inner	0.3202
Outer	0.3922

Table 2. Modeled Parameters for the Fresh Nuclear Fuel.

Fuel density	10.339 g/cm^3
Fuel rod radius	0.3922 cm
Inner radius of cladding	0.4000 cm
Outer radius of cladding	0.457 cm
Fuel rod length	365.8 cm
Fuel pitch	1.26 cm
Fuel assembly lattice	17×17

Table 3. Composition of Simulated UO_2 Fuel Rod.

Isotope	Atomic fraction
^{16}O	6.667E-01
^{235}U	1.100E-02
^{238}U	3.223E-01
^{244}Cm	3.333E-37

Table 4. Composition of the Zircaloy Cladding Modeled. Mass Density is 6.3902 g/cm3.

Element	Atomic fraction
^{90}Zr	4.989E-01
^{91}Zr	1.088E-01
^{92}Zr	1.663E-01
^{94}Zr	1.685E-01
^{96}Zr	2.715E-02
^{112}Sn	1.181E-04
^{114}Sn	7.916E-05
^{115}Sn	4.384E-05
^{116}Sn	7.734E-03
^{117}Sn	9.353E-04
^{118}Sn	2.950E-03
^{119}Sn	1.045E-03
^{120}Sn	3.969E-03
^{121}Sn	5.638E-04
^{122}Sn	7.051E-04
^{54}Fe	2.148E-04
^{56}Fe	3.339E-03
^{57}Fe	7.645E-05
^{58}Fe	1.019E-05
^{50}Cr	9.438E-05
^{52}Cr	1.820E-03
^{53}Cr	2.064E-04
^{54}Cr	5.137E-05
^{16}O	5.366E-03
C	9.027E-04

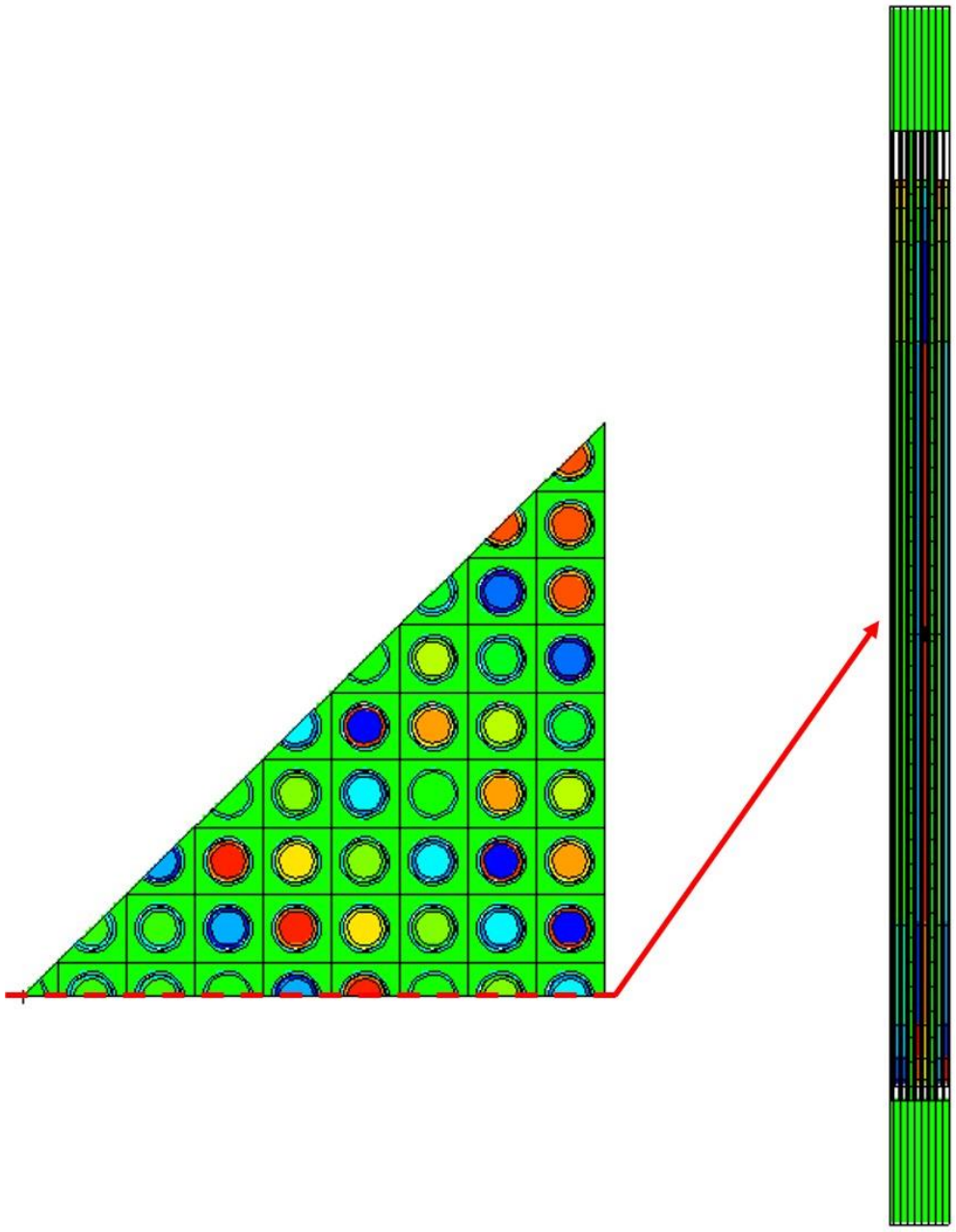

Figure 2. Visualization of the One-eighth PWR Fuel Assembly Model Prepared Using MCNP6 code. (There are 27 complete fuel rods, 12 half fuel rods. In addition, 1 complete water hole, 4 half water holes, and 1 one-eighth water hole are placed in the fuel assembly.)

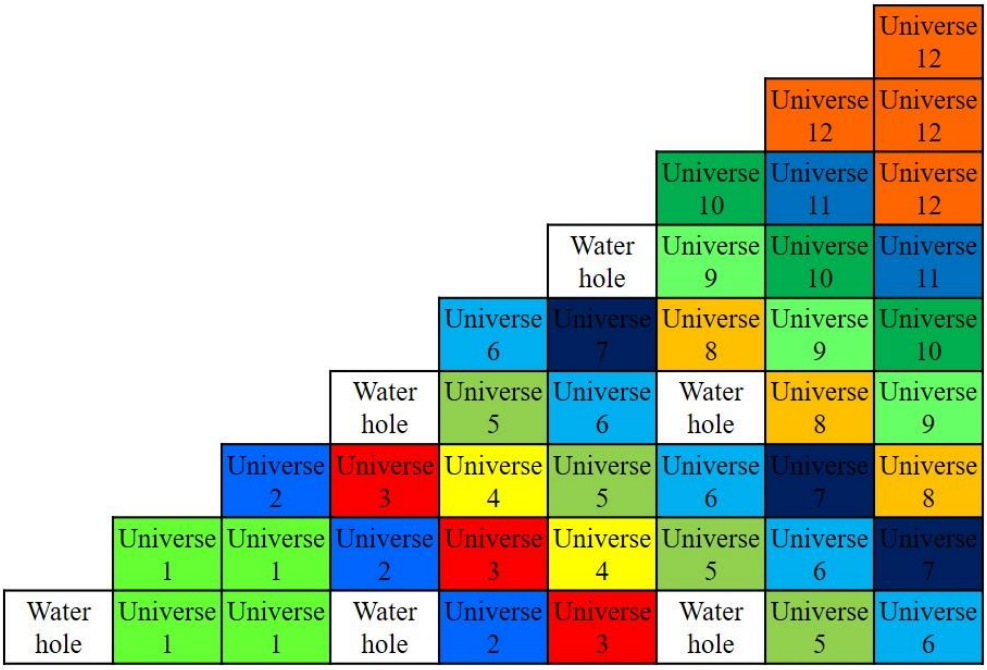

Figure 3. Arrangement of the Universes Designed and the Water Holes.

Sampling from the Head-end Processes

Chopping Process

The fuel assembly length is 365.8 cm, so it is not suitable to be fed as a single material for pyroprocessing because it does not provide good surface area for converting into a molten form. Therefore, it should be split into small pieces to be used as a feed material. The chopping process is designed for this purpose. However, the length of the chopped piece of the used fuel has not been decided yet. In this project, 1 cm length is assumed as a length of a chopped piece. Since the length of a fuel rod is 365.8 cm, there are also chopped pieces of 0.8 cm after chopping process. As a result, there are 96,624 chopped pieces, which is obtained from the chopping process.

As described previously, the radial non-uniformity of nuclide composition in chopped pieces is not important for this project, the nuclide composition such as Pu and ^{244}Cm is averaged along the radial direction. In order to measure the uncertainties of the Pu-to-^{244}Cm ratio of samples

taken from the chopping process, 5 cases of varying samples sizes, 10, 20, 30, 50, and 100 chopped pieces, are applied. These sampling trials are repeated 10,000 times for each sampling case. The uncertainties of the Pu-to-^{244}Cm ratio are then calculated by the propagation of errors using the standard deviation of the mass density for Pu and ^{244}Cm.

Voloxidation Process

As mentioned above, the voloxidation process is utilized to convert UO_2 to U_3O_8 by which undergoes the following reaction, $3UO_2 + O_2 \rightarrow U_3O_8$ [2]. In order to obtain the uncertainties of the Pu-to-^{244}Cm ratio for samples from the voloxidation process, U_3O_8 powder size should be first decided. The powder size distribution data is extracted from the reference paper published by Song as shown in Figure 4[13]. Then, the type of distribution is decided to be used for the study. Therefore, the normality of the extracted distribution is tested by using below Eq. 4 of Jarque-Bera (JB) test[16].

$$JB = \frac{n-k+1}{6}\left(S^2 + \frac{1}{4}(C-3)^2 \right) \qquad \text{Eq. 4}$$

Where,

JB= Jarque-Bera test score

n= number of observations

k= number of regressors

S= sample skewness

C= sample kurtosis

The sample skewness (*S*) and the sample kurtosis (*C*) are computed by using below Eq. 4-1 and 4-2.

$$S = \frac{\frac{1}{n}\sum_{i=1}^{n}\left(x_i - \bar{x}\right)^3}{\left(\frac{1}{n}\sum_{i=1}^{n}\left(x_i - \bar{x}\right)^2\right)^{\frac{3}{2}}} \qquad \text{Eq. 4-1}$$

$$C = \frac{\frac{1}{n}\sum_{i=1}^{n}\left(x_i - \bar{x}\right)^4}{\left(\frac{1}{n}\sum_{i=1}^{n}\left(x_i - \bar{x}\right)^2\right)^2} \qquad \text{Eq. 4-2}$$

By using the above equations, if the distribution is a log-normal distribution, JB test score is calculated as 2.51, which is less than the critical score 5.991. Therefore, it is found that the referred distribution follows the log-normal distribution. The graphical view of the extracted distribution and the actual log-normal distribution is shown in Figure 5.

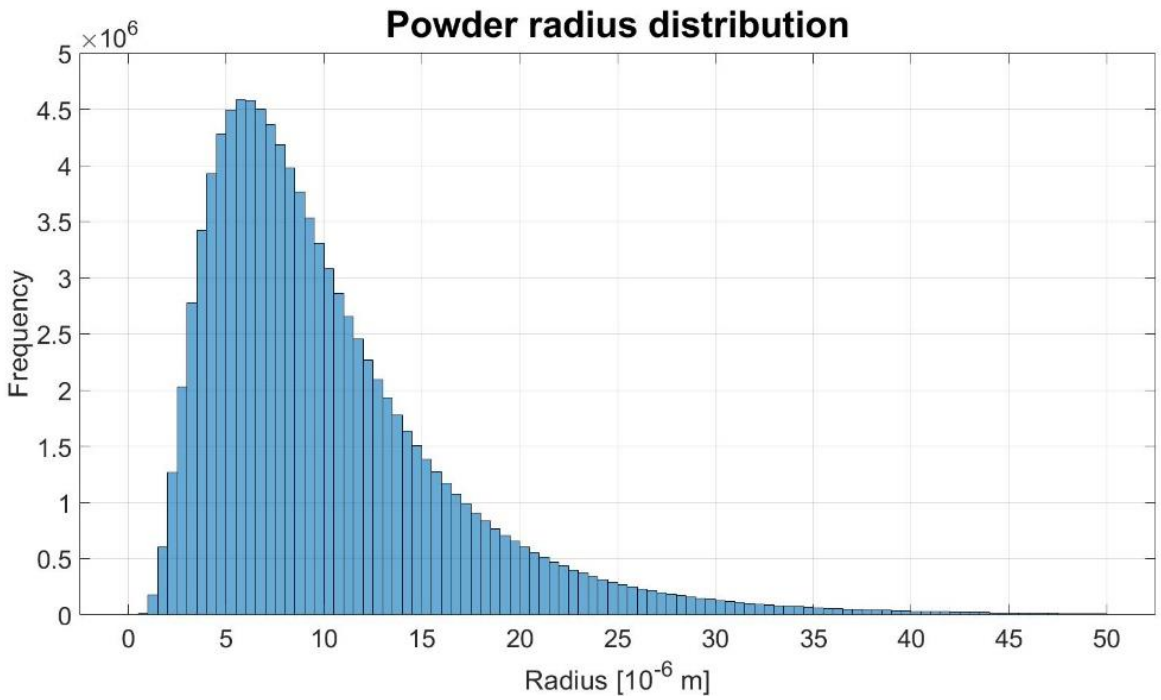

Figure 4. U_3O_8 Powder Size Distribution Extracted from the Reference[13].

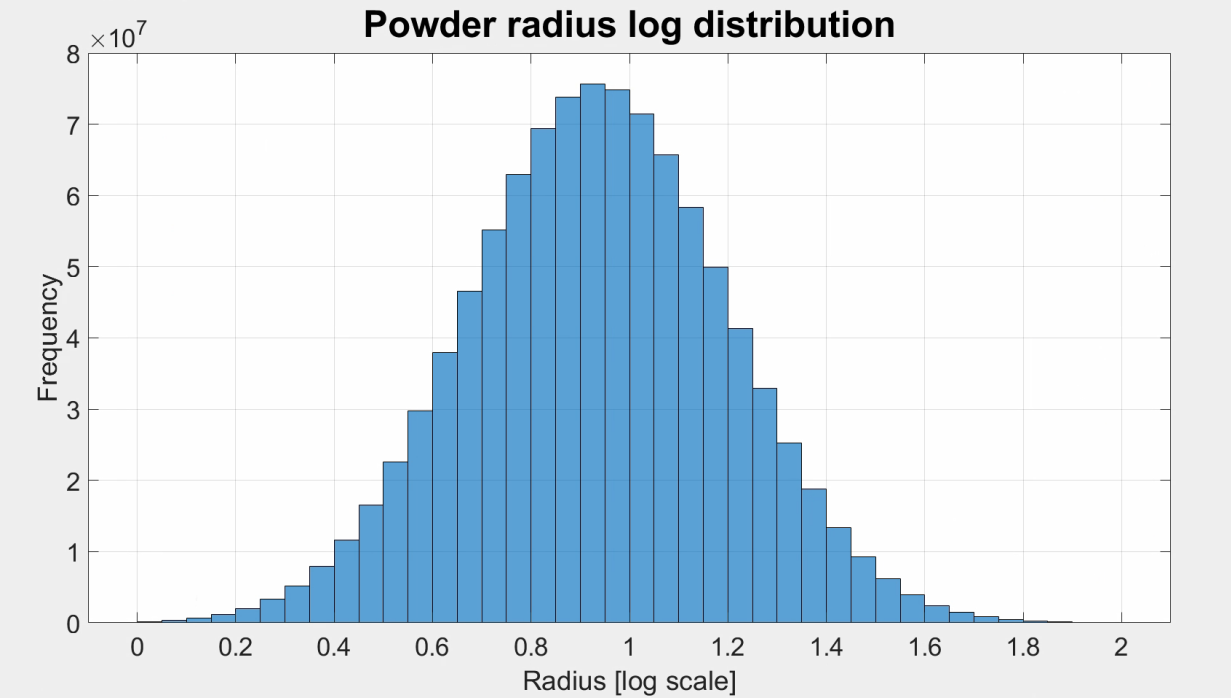

Figure 5. Comparison between Distribution of Extracted U_3O_8 Powder Size in Log Scale and the Actual Log-normal Distributions

By using the obtained distribution, which follows a log-normal distribution, U_3O_8 powders can be randomly sampled from products of the voloxidation process. The composition of the used nuclear fuel has already been obtained by the depletion calculation using MCNP6 code, so the uncertainty of the Pu-to-^{244}Cm ratio can be estimated by applying IAEA's International Target Value (ITV) of DA method for randomly sampled powders. More specifically, 3 lab spoon sizes, 0.05 ml, 0.1 ml, and 0.5 ml are assumed. The assumed lab spoon is used to take samples of U_3O_8 powders processed by voloxidation. Sampling powders from the obtained powder size distribution using MATLAB code is then repeated until the cumulative volume of sampled powders reaches the assumed volume of the lab spoon. When the cumulative volume of sampled powders reaches the lab spoon's volume, sampling is finished. Pu and ^{244}Cm contents in sampled powders can then be obtained. It means that the Pu-to-^{244}Cm ratio in voloxidation process is also estimated.

Pu-to-^{244}Cm Ratio Method

As explained, the Pu-to-^{244}Cm ratio is a kind of measurements to estimate Pu in a used fuel by assuming that ^{244}Cm is a dominant neutron source in used spent fuel. The SF yields[17] for various neutron sources including Pu and ^{244}Cm are listed in Table 5. The most active isotope among Pu isotopes is ^{238}Pu which has 2.59E+03 n/s-g of SF yield. The ^{244}Cm, however, emits about 4200 times more neutrons than ^{238}Pu. Therefore, if the Pu-to-^{244}Cm ratio is assumed as the known factor and the amount of ^{244}Cm at any desired step is measured, the amount of Pu can be also estimated.

Table 5. Spontaneous Fission Neutron Yields. (These yields are referred from the paper[17].)

Isotope	Half-life [yr]	SF yield [n/s-g]	SF multiplicity
^{237}Np	2.14E+06	1.14E-04	2.05
^{238}Pu	8.77E+01	2.59E+03	2.21
^{239}Pu	2.41E+04	2.18E-02	2.16
^{240}Pu	6.56E+03	1.02E+03	2.16
^{241}Pu	1.44E+01	5.00E-02	2.25
^{242}Pu	3.76E+05	1.72E+03	2.15
^{244}Cm	1.81E+01	1.08E+07	2.72

For this study, the Pu-to-^{244}Cm ratios with their uncertainties depending on two sampling sources which are the chopped nuclear fuel rod and the voloxidized powders are evaluated first. Then, the amount of Pu for various sampling schemes after the used fuel assembly is processed by the key-pyroprocess is computed by multiplying the Pu-to-^{244}Cm ratio with the measured amount of ^{244}Cm. The half-life of ^{244}Cm is 1.81E+01 years as shown in Table 15, so it has not impact on this research, because it is assumed that used fuel assembly is processed just after 5 years of cooling time. The amount of ^{244}Cm in TRU can be estimated by Passive Well Coincidence Counter

(PWCC)[18,19]. The PWCC is one of the neutron detectors which can measure spontaneous fission neutrons from a target material. The PWCC system usually consists of 42 ^{3}He tubes covered by polyethylene moderators[20]. This detector obtains the neutron double count rates mostly emitted from ^{244}Cm. By using this measured neutron doubles count rate, the amount of ^{244}Cm in a target material such as TRU ingot in the pyroprocessing facility can be calculated using Eq. 5[21].

$$D = \frac{F_0 \cdot {}^{244}Cm_{eff} \cdot \varepsilon^2 \cdot f_d \cdot M_L^2}{2} \times \left[\nu_{s2} + \left(\frac{M_L - 1}{\nu_{i1} - 1} \right) \cdot \nu_{s1} \cdot \nu_{i2} \right] \quad \text{Eq. 5}$$

Where,

D= the doubles count rate

F_0= the specific spontaneous fission neutron emission rate for ^{244}Cm

$^{244}Cm_{eff}$= the mass of ^{244}Cm

ε= the detector efficiency

f_d= the doubles gate fraction

M_L= the leakage multiplication factor

ν_{s1}, ν_{s2}= the 1st and 2nd moments of the spontaneous fission neutron distribution

ν_{i1}, ν_{i2}= the 1st and 2nd moments of the induced fission neutron distribution.

MUF and Sigma-MUF Calculations

MUF for a MBA over a MBP is calculated using Eq. 6[8]. In addition, σ_{MUF} can be estimated using Eq. 6-1.

$$\mathrm{MUF} = (\mathrm{PB} + \mathrm{X} - \mathrm{Y}) - \mathrm{PE} \quad \text{Eq. 6}$$

$$\sigma_{\mathrm{MUF}} = \sqrt{\sigma_{\mathrm{PB}}{}^2 + \sigma_{\mathrm{X}}{}^2 + \sigma_{\mathrm{Y}}{}^2 + \sigma_{\mathrm{PE}}{}^2} \quad \text{Eq. 6-1}$$

Where,

PB= beginning physical inventory

X= sum of increases to inventory

Y= sum of decreases from inventory

PE= ending physical inventory

The Pu mass of used nuclear fuel has been determined by MCNP6 code depletion simulation. Moreover, the Pu-to-^{244}Cm ratios in both chopping and voloxidation process are obtained by MATLAB calculation as explained above. Therefore, the Pu content after the key-pyroprocess can be also computed by using NDA technique[5] which measures ^{244}Cm mass in processed products from pyroprocess. By multiplying the Pu-to-^{244}Cm ratio and measured ^{244}Cm mass, Pu mass is computed. MUF is then estimated by computing Pu contents before and after the used fuel is processed.

The σ_{MUF} can be also computed since Pu content and the uncertainties of Pu-to-^{244}Cm ratios have been obtained. For a more reliable study, ITVs for DA and NDA methods used to measure Pu and ^{244}Cm at the Key Measurement Point (KMP) in the pyroprocess facility are assumed. Therefore, the Pu uncertainties, which are originated from the non-uniformity of used fuel and ITVs are propagated to calculate σ_{MUF}.

CHAPTER III

RESULTS

MCNP Predicted Nuclide Compositions in Used Fuel and Stochastic Uncertainties

As it was mentioned in Chapter II, the data on nuclide compositions obtained from the fuel burnup calculation by MCNP6 code should be verified to confirm that the non-uniformity of nuclide compositions are real and not due to the stochastic variations because of the inherent nature of Monte Carlo solution methodology employed in the code. A dominant path of ^{239}Pu production during fuel irradiation in the reactor core is $^{238}_{92}\mathrm{U} \xrightarrow{(n,\gamma)} {}^{239}_{92}\mathrm{U} \xrightarrow{\beta^-} {}^{239}_{93}\mathrm{Np} \xrightarrow{\beta^-} {}^{239}_{94}\mathrm{Pu}$, where β^- represents the decay of the isotope through beta decay.

Therefore, the MCNP predicted stochastic uncertainties of ^{238}U capture reaction rate in all the meshes in the fuel assembly model used should be less than the non-uniformity of Pu content. The non-uniformity of Pu, which is defined for this study is calculated using Eq. 7.

$$R = \frac{D_{Pu_n} - D_{Pu_{n+1}}}{D_{Pu_n}} \qquad \text{Eq. 7}$$

Where,

R= non-uniformity of Pu

D= mass density of ^{239}Pu

n= nth mesh

Based on the MCNP predicted results, the non-uniformity in nuclide compositions are found to be greater than the stochastic uncertainties. Therefore, it can be considered that the depletion simulation using MCNP6 is reliable. In other words, the nuclide compositions of a used nuclear

fuel obtained by the simulation show the actual non-uniformity and not due to the stochastic nature of the MCNP6 code.

Composition Change in Nuclear Fuel during Fuel Burnup

As the simulated fuel assembly gets burned in the reactor core the change in nuclide composition in the fuel predicted by MCNP6 code are shown in Figures 6, 7, 8, and 9. The composition of important nuclides in one-eighth used fuel assembly after 986 days of irradiation and 5 years of cooling time is listed in Table 6. Total Pu gradually increases as the fuel burnup increases. Initially, ^{239}Pu is rapidly produced than other isotopes. This is because of the Pu production chain shown in Figure 10. Fresh nuclear fuel consists of ^{238}U mostly. Once the fuel starts burning in the reactor core, ^{238}U captures a neutron and becomes ^{239}U which has 23.5 minutes of half-life. Because of the beta decay of ^{239}U, ^{239}Pu is produced. After ^{239}Pu is produced, ^{240}Pu, ^{241}Pu, and ^{242}Pu are produced in a row as neutrons are captured by lighter Pu isotopes. In addition, ^{238}Pu is a decay product of ^{242}Cm (α decay), ^{238}Am (β^+ decay), and ^{238}Np (β^+ decay), which are also produced after ^{238}U gets burned.

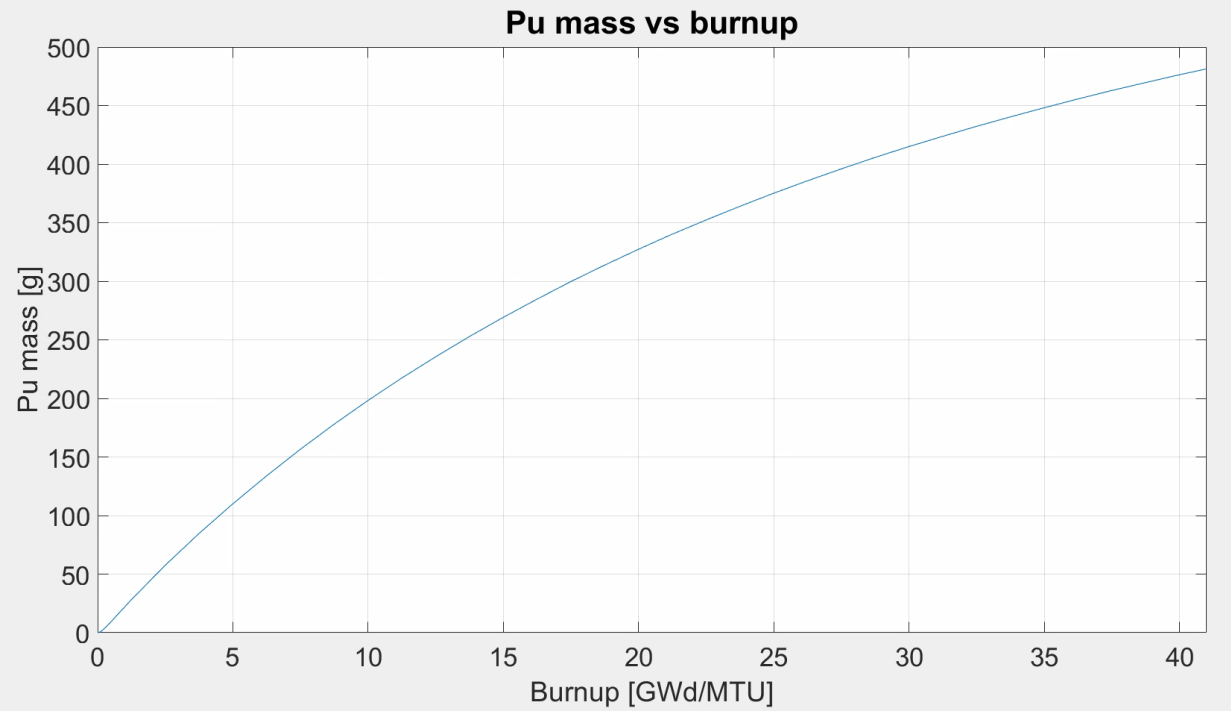

Figure 6. Sum of Pu Isotopes Mass Including ^{238}Pu, ^{239}Pu, ^{240}Pu, ^{241}Pu, and ^{242}Pu as a Function of Fuel Burnup.

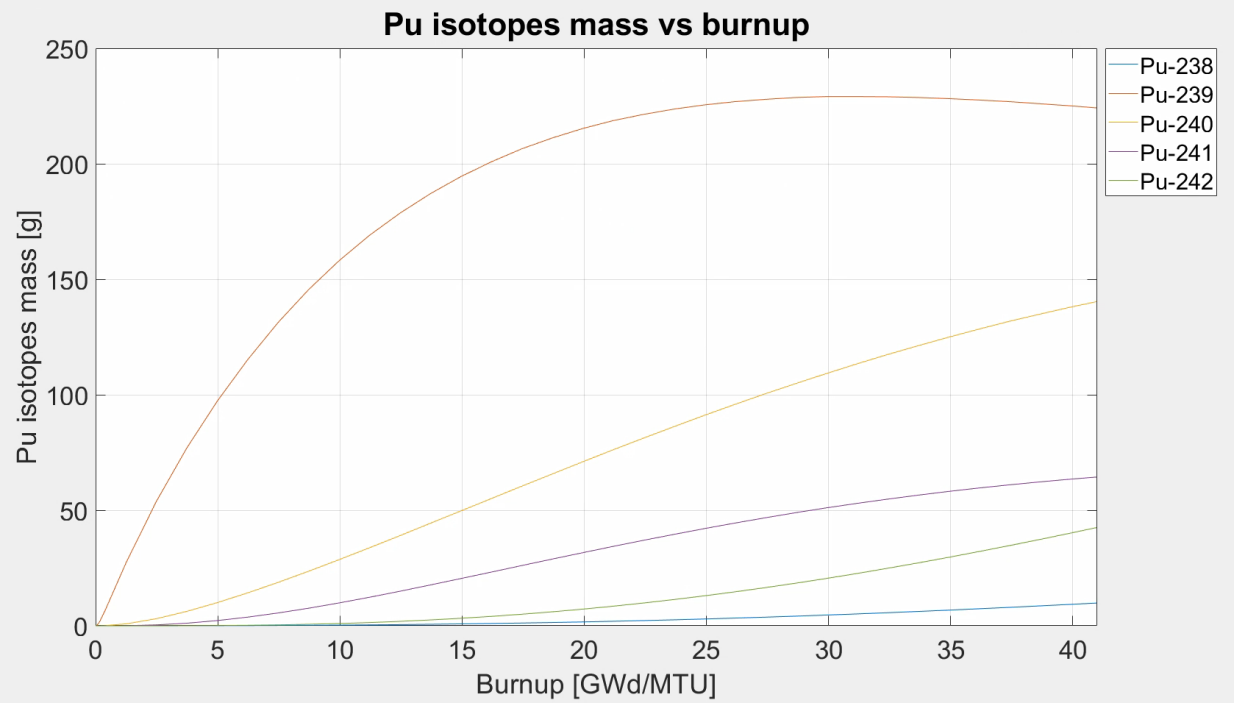

Figure 7. Mass for Each Pu Isotope as a Function of Fuel Burnup.

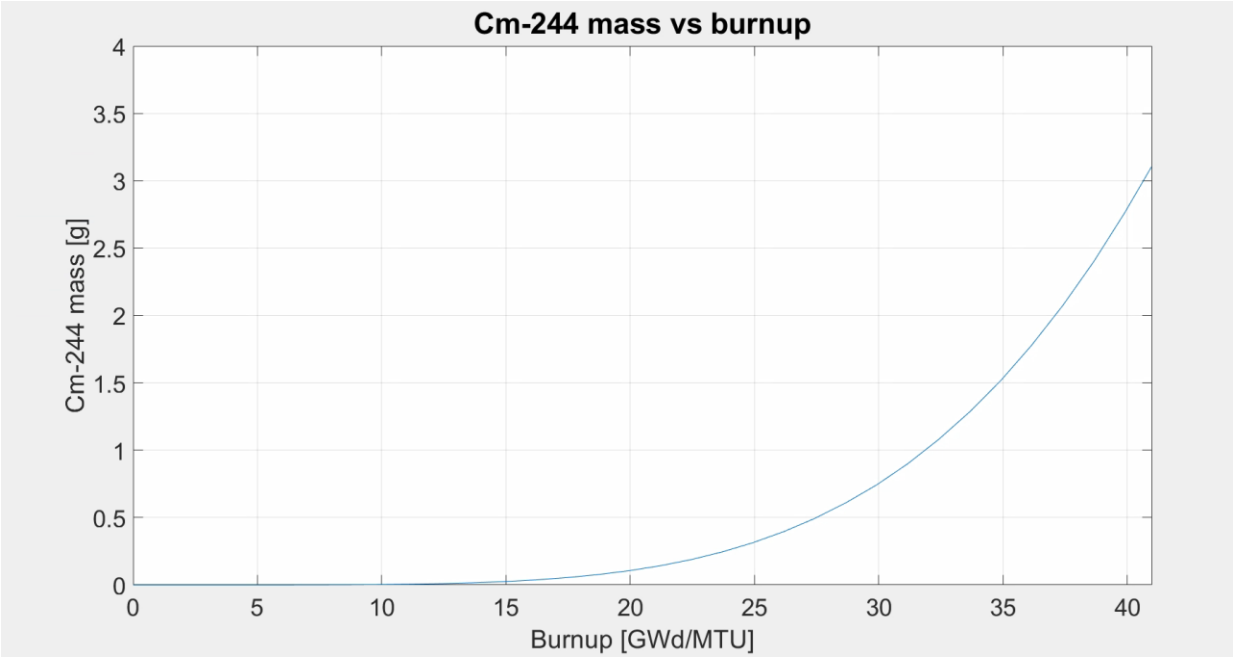

Figure 8. ^{244}Cm Mass as a Function of Fuel Burnup.

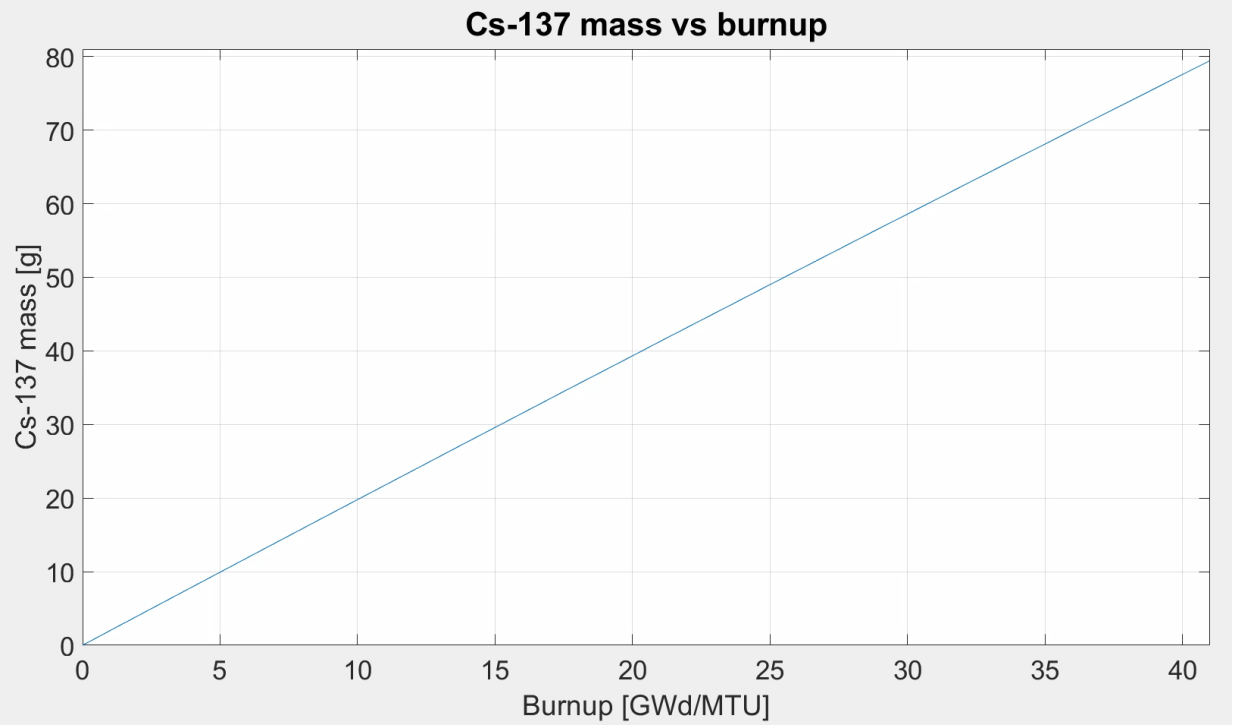

Figure 9. ^{137}Cs Mass as a Function of Fuel Burnup.

$$^{238}_{92}\mathrm{U} \xrightarrow{(n,\gamma)} {}^{239}_{92}\mathrm{U} \xrightarrow{\beta^-} {}^{239}_{93}\mathrm{Np} \xrightarrow{\beta^-} {}^{239}_{94}\mathrm{Pu} \xleftarrow{(n,\gamma)} {}^{238}_{94}\mathrm{Pu}$$

$$\downarrow (n,\gamma)$$

$$^{240}_{94}\mathrm{Pu} \xrightarrow{(n,\gamma)} {}^{241}_{94}\mathrm{Pu} \xrightarrow{(n,\gamma)} {}^{242}_{94}\mathrm{Pu}$$

Figure 10. Production Chain for Pu.

^{244}Cm has a different decay chain as shown in Figure 11[22]. ^{244}Cm is produced in noticeable amounts after 10 GWd/MTU, where ^{241}Pu and ^{242}Pu begin to be produced enough. More specifically, the production of ^{244}Cm is strongly affected by the production of ^{241}Pu and ^{242}Pu as shown in Figure 10.

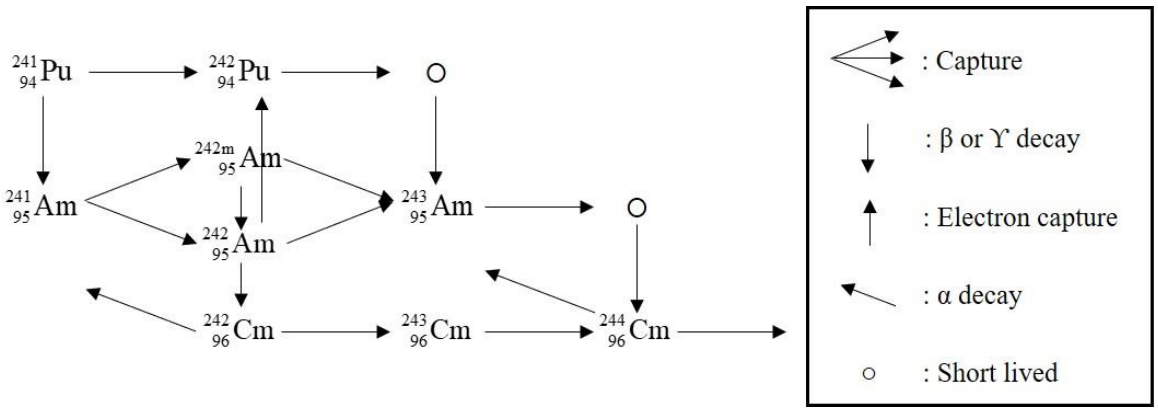

Figure 11. Production Chain for ^{244}Cm. (This is referred from the literature paper[22].)

Isotopes mentioned above such as Pu and ^{244}Cm increase nonlinearly as the fuel gets burned. However, ^{137}Cs increases linearly unlike other isotopes as shown in Figure 9. This is a very important feature of the fuel depletion for nuclear material safeguards approaches. In other words, because of this linear relation between ^{137}Cs and burnup, IAEA inspectors can determine the burnup of fuel indirectly by using easily measurable ^{137}Cs. Moreover, ^{137}Cs buildup trend as a function of fuel burnup is used to verify that the data from MCNP6 is reliable with respect to continuous burnup. If there were any errors during MCNP simulation, this relationship would not be linear.

Table 6. Important Nuclide Composition Obtained from MCNP6 Simulations in One-eighth Used Fuel Assembly after 986 Days of Irradiation and 5 Years Cooling Time.

Isotope	Mass [g]
^{238}Pu	1.041E+01
^{239}Pu	2.302E+02
^{240}Pu	1.408E+02
^{241}Pu	5.057E+01
^{242}Pu	4.250E+01
^{244}Cm	2.569E+00

Non-uniformity of Nuclide Composition in Used Fuel

Axial Distribution for Pu and ^{244}Cm

Nuclide composition variation is due to the axial variation of the moderator (water) temperature, neutron flux and the proximity of fuel rods to the water holes even though all fuel rods have same dimensions, uranium content and uranium enrichment.

The axial distribution for Pu mass density after 986 days of irradiation and 5 years of cooling time is plotted in Figure 12. In Figure 12, the axial location of mesh in a fuel rod is shown on the x-axis, from bottom to the top of the rod. The average, the maximum, and the minimum mass densities of Pu are 8.13E-2 g/cm^3, 8.70E-2 g/cm^3, and 4.84E-2 g/cm^3. The maximum Pu mass density is about 1.8 times greater than the minimum value. In addition, the average value is close to the maximum value than the minimum Pu mass density. The peaking of Pu mass density is in mesh at 320 cm at the universe 12 as shown in Figure 12. This peaking is hence located close to the top of the fuel rod than the middle. This is because the largest isotope in a used fuel assembly is ^{239}Pu as mentioned previously. The mass density of ^{239}Pu is highly affected by the axial neutron flux distribution because there is only one step between ^{238}U and ^{239}Pu, which means ^{239}Pu is

produced by only one capture reaction of ^{238}U. The axial neutron flux distribution of a used fuel assembly peaks at about 80% from the bottom of a fuel rod[23]. This is because ^{235}U in the lower axial area are burned more than that in the upper area at the beginning of the burnup since the water density of that area is higher. It means more neutrons are moderated to be easily captured in the lower area. Therefore, the peaking of the axial neutron flux is located close to the bottom of the fuel rod at the beginning of the burnup. However, as fuel gets burned, the peaking of the axial neutron flux is moved toward the top of the fuel rod since more ^{235}U exist in the upper axial area of the fuel rod. In other words, the axial neutron flux peaks near the top of the fuel rod at the end of the burnup. Therefore, the peaking of Pu is similar to that of the axial neutron flux distribution that the peaking is located close to the top.

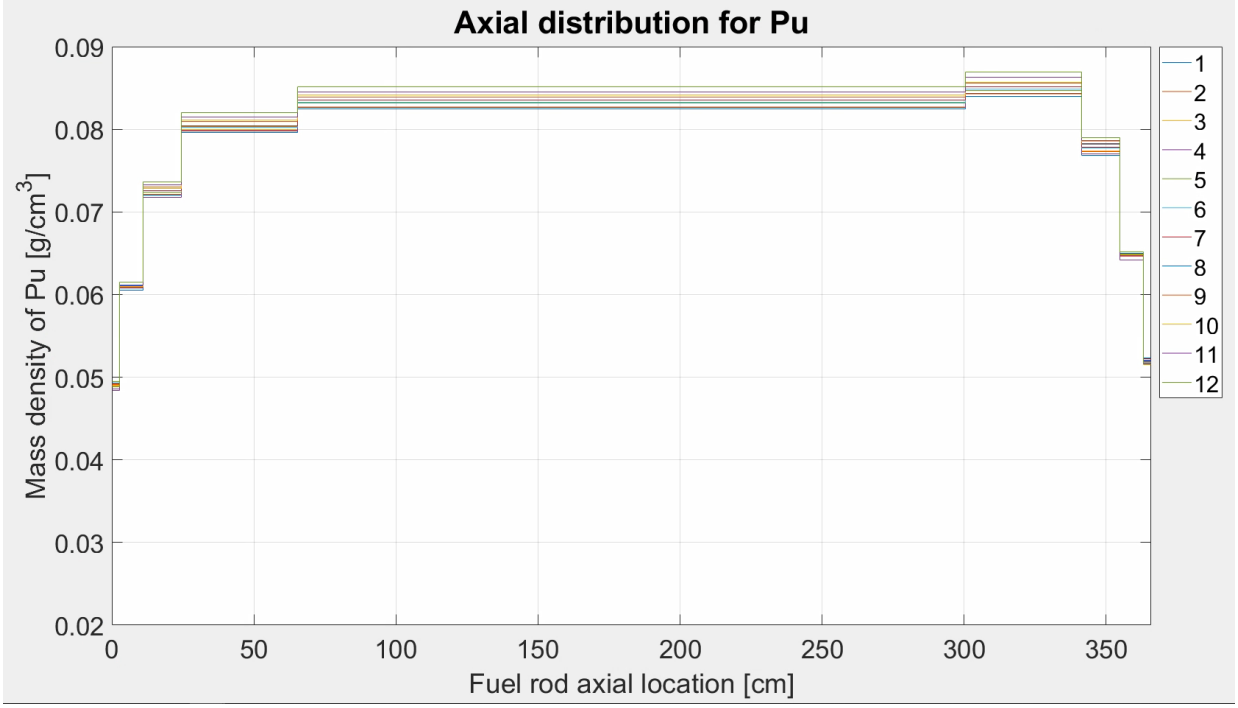

Figure 12. Pu Mass Density as a Function of Axial Location of a Fuel Rod. (Legend indicates the universe of the fuel rod.)

The axial distribution for ^{244}Cm in the used nuclear fuel after 986 days of irradiation and 5 years cooling time is shown in Figure 13. The maximum value is 5.60E-4 g/cm^3 at the middle of the fuel rod in universe 2. The minimum value of ^{244}Cm is 1.92E-5 g/cm^3 and is at the bottom of the fuel rod for the universe 12. The average ^{244}Cm mass density is 4.40E-4 g/cm^3. The maximum value is about 30 times greater than the minimum value. Compared with the case for the axial distribution for Pu mass density, the difference between the maximum and the minimum value for ^{244}Cm mass density is much more significant. This is due to the fact that the slope of the Pu production curve gets flat as the burnup increases because the loss of ^{239}Pu becomes significant as shown in Figure 7. This means that the axial distribution of Pu in fuel rods gets smaller as time goes by. Unlike Pu, however, the ^{244}Cm production curve gets steeper as fuel gets burned as shown in Figure 8. Therefore, the difference between the maximum mass density and the minimum mass density for ^{244}Cm is more significant than that of Pu.

Moreover, the peaking of ^{244}Cm is located at the middle axial mesh of the fuel rod. ^{244}Cm is generated through several decay chains from ^{241}Pu which is produced by the capture reaction of ^{240}Pu as described in Figure 11. It means that the axial distribution for ^{244}Cm would be more similar to that of ^{240}Pu and ^{241}Pu than that of ^{239}Pu. In other words, there is a kind of time delay effect due to this. Therefore, the peaking of ^{244}Cm is located in the middle as if the peaking of the neutron flux is located in the middle of the fuel rod when the middle burnup. If the ^{244}Cm peaking at the later burnup such as 50 GWd/MTU is plotted, it would be located close to the top of the fuel rod since enough time is elapsed. This is the reason why the shape of the axial distribution for Pu is different from that of ^{244}Cm at 42 GWd/MTU.

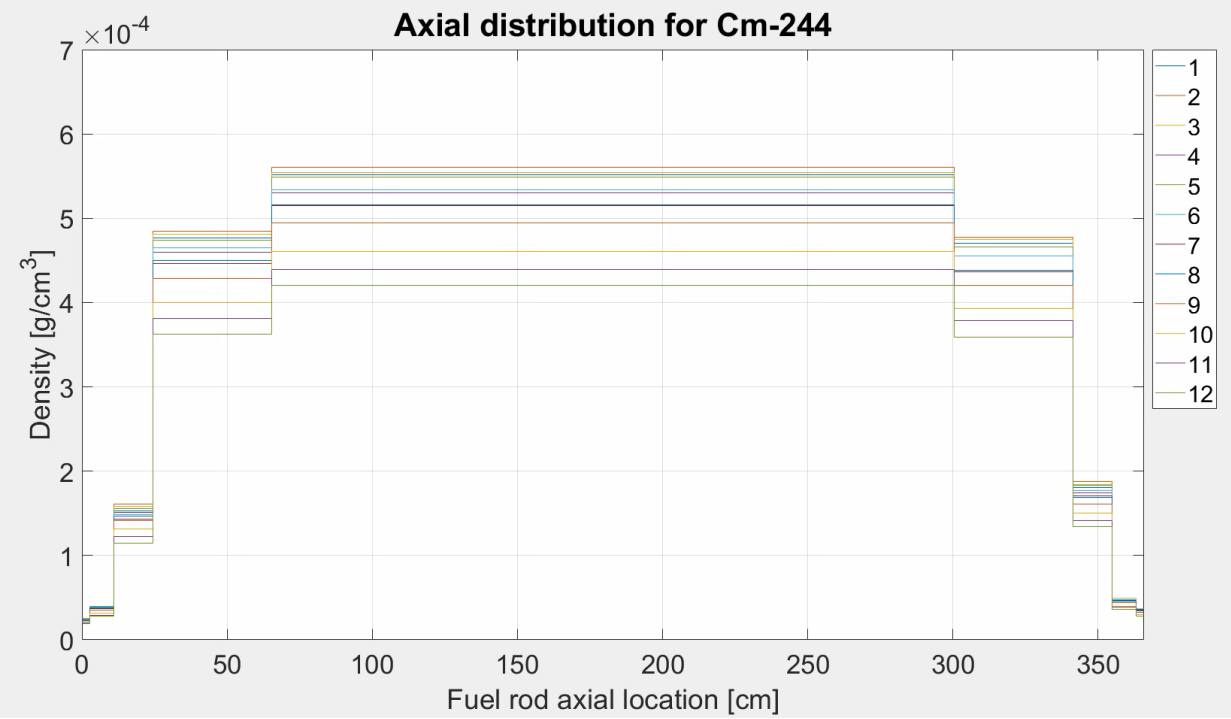

Figure 13. ^{244}Cm Mass Density as a Function of Axial Location of a Fuel Rod. (Legend indicates the universe of the fuel rod.)

Finally, the axial distribution for the Pu-to-^{244}Cm ratio is shown in Figure 14. The maximum value is 2,544 at the bottom of the fuel rod for the universe 12. The lowest ratio is 147.54 at the middle of the fuel rod for the universe 2. The greatest ratio is about 17 times higher than the lowest value. This difference could lead to a negative effect on NMA of Pu in a pyroprocessing facility if the measurement samples of fuel powder are taken inappropriately. For instance, if a sample is only taken from the top of the used fuel rod to obtain the Pu-to-^{244}Cm ratio, the Pu calculated by the Pu-to-^{244}Cm ratio method after used fuel assemblies are processed will be an overestimate.

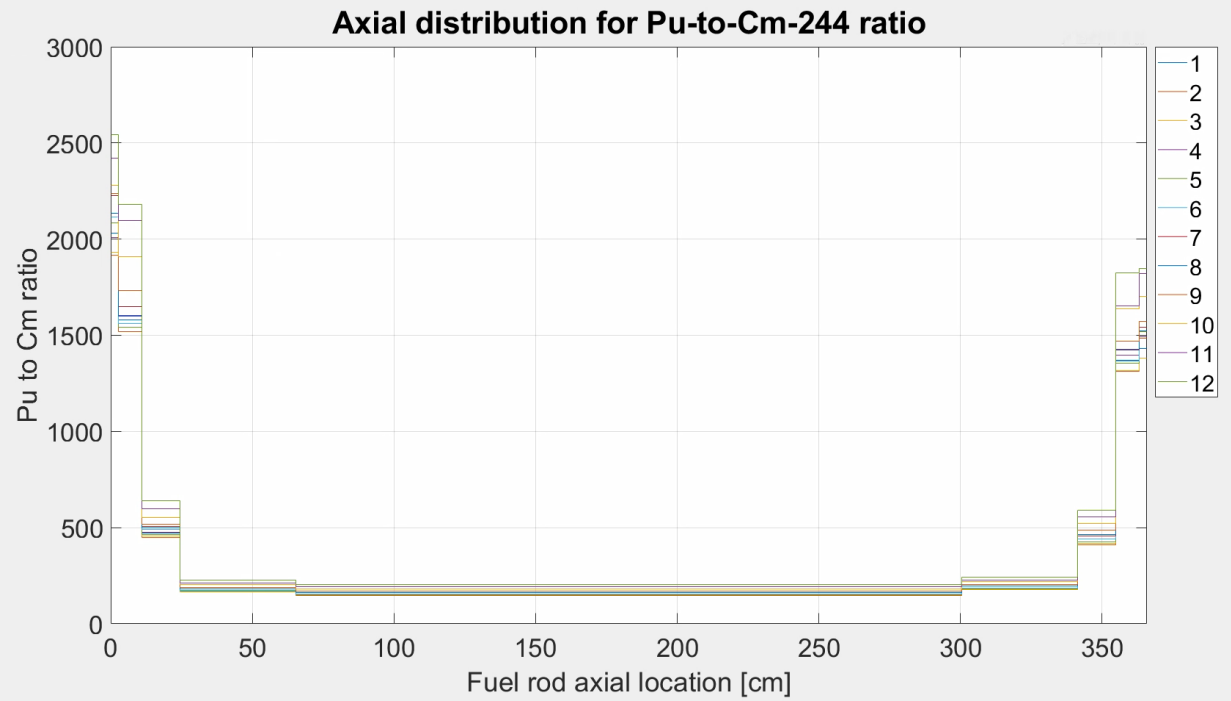

Figure 14. Pu-to-^{244}Cm Ratio as a Function of Axial Location of a Fuel Rod. (Legend indicates the universe of the fuel rod.)

Radial Distribution for Pu and ^{244}Cm

There is also the radial distribution of the nuclide composition in the used fuel in addition to the axial distribution. In order to investigate the radial distribution, the mass densities of Pu and ^{244}Cm and the Pu-to-^{244}Cm ratio at the universe 2 as a function of the fuel rod radius are shown in Figures 15, 16 and 17. As shown in Figure 15, the Pu mass density is higher at the outer radial mesh. The largest Pu mass density is 2.10E-1 g/cm^3 at the 6th axial mesh of the outer radial mesh. The minimum value is 0.088 g/cm^3 at the inner radial mesh in the bottom of the fuel rod. The maximum value is about 2.3 times greater than the lowest value. The radial distribution can be caused by the rim effect of the fuel rod[24]. It means that many neutrons are captured by ^{238}U at the outer layer of the fuel rod (self-shielding effect). Therefore, Pu is produced more at the outer mesh

than in the nuclear fuel region at the inner radial mesh. Moreover, Pu is produced less near the bottom and the top of the fuel rod. This is attribute to the fact that the surfaces of the top and the bottom of the fuel rod are also affected by the rim effect. In addition to this, the leakage of neutrons happens at the top and the bottom of the fuel rod even though water reflectors are placed.

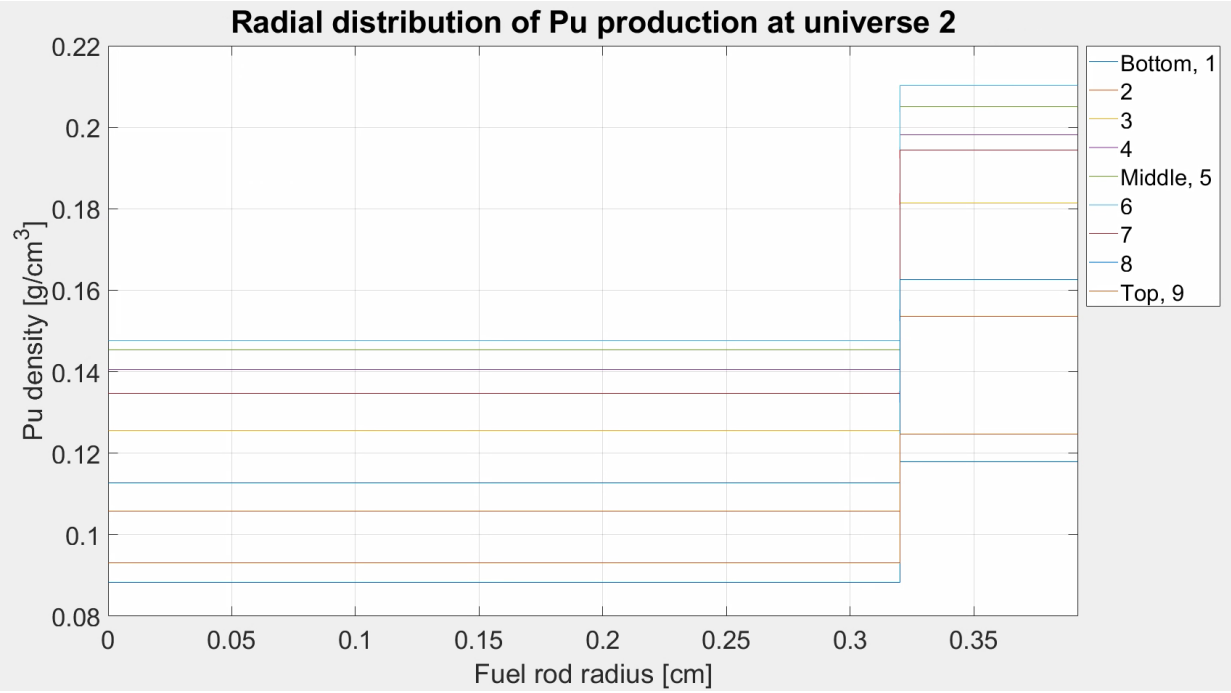

Figure 15. Pu Mass Density as a Function of Radial Location of a Fuel Rod at the Universe 2. (Legend indicates an axial location of a fuel rod.)

Similar to the radial distribution of Pu discussed above, ^{244}Cm mass density also shows the radial distribution as shown in Figure 16. The maximum mass density of ^{244}Cm is 1.60E-3 g/cm^3 at the outer radial mesh in the middle of the fuel rod. The minimum value is 4.29E-5 g/cm^3 at the inner layer in the bottom of the fuel rod. The greatest value is approximately 37 times greater than the minimum value. This difference is more significant than that of Pu. The rim effect is responsible for these radial distribution variations.

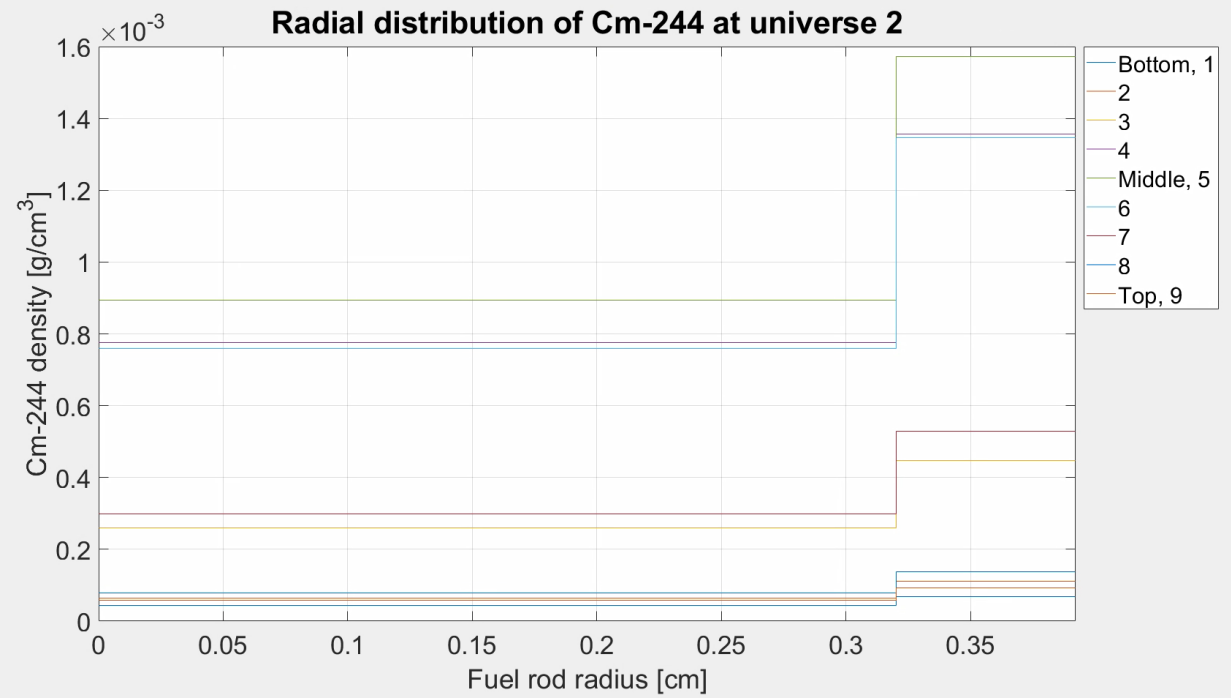

Figure 16. ^{244}Cm Mass Density as a Function of Radial Location of a Fuel Rod at the Universe 2. (Legend indicates an axial location of a fuel rod.)

Since both Pu and ^{244}Cm mass density show the radial distribution mentioned above, it is obvious to see a similar radial distribution for the Pu-to-^{244}Cm ratio, which is shown in Figure 17. The maximum value is 2,058 at the inner layer in the bottom of the fuel rod. The minimum ratio is 130.34 at the outer layer in the middle of the fuel rod. This radial distribution is not important to the chopping process since Pu and ^{244}Cm in samples taken from the chopping process are axially averaged. However, if samples are taken from the voloxidation process, this radial distribution can lead to a negative effect on the estimation of Pu in pyroprocessing NMA. Therefore, this radial distribution of the Pu-to-^{244}Cm ratio should be appropriately accounted for in NMA at a pyrprocessing facility.

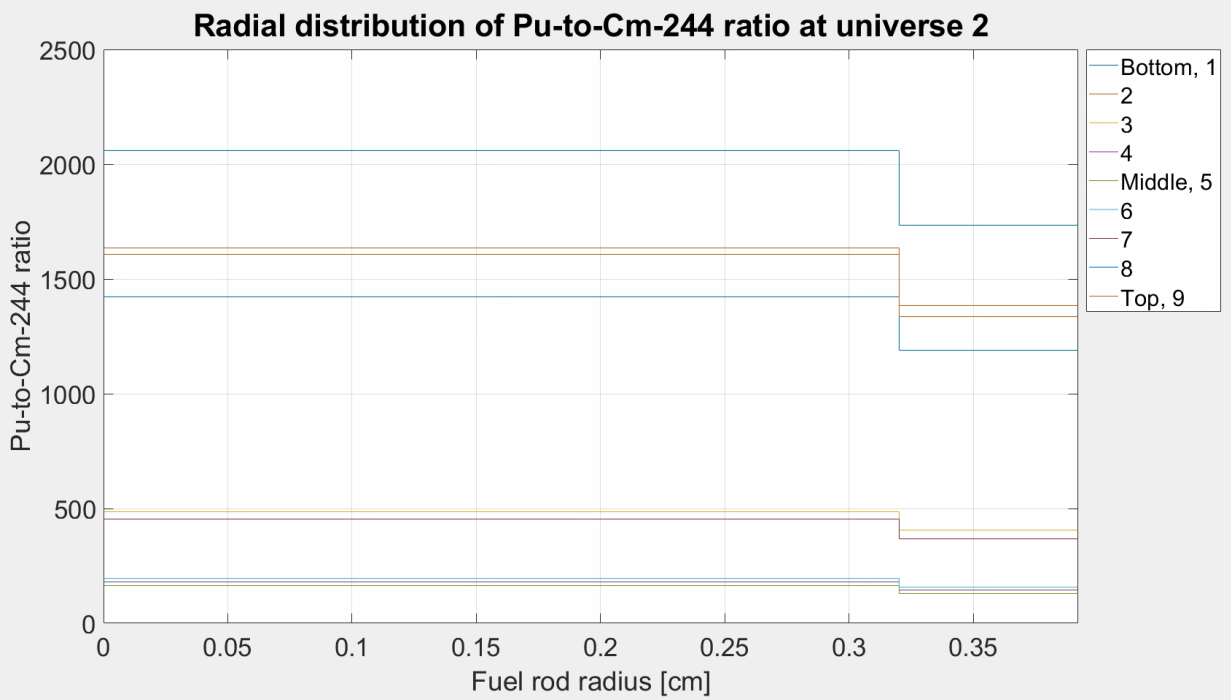

Figure 17. Pu-to-^{244}Cm Ratio as a Function of Radial Location of a Fuel Rod at the Universe 2. (Legend indicates an axial location of a fuel rod).

Statistical Analysis to Determine Non-uniformity of Nuclide Compositions in Used Fuel

Chopping Process

The mass densities of Pu and ^{244}Cm for 96,624 chopped pieces at the pyroprocess head-end step for one used fuel assembly are plotted in Figures 18 and 19. Most chopped pieces are in 1 cm length and only 264 pieces are in 0.8 cm length and the length of a fuel rod is 365.8 cm. As expected, the axial distribution of Pu and ^{244}Cm presented earlier provides the reason for the variations of mass densities of Pu and ^{244}Cm in chopped pieces. Because of these variations of chopped pieces from the chopping process, it is expected that the Pu-to-^{244}Cm ratio would be varied when samples are taken randomly. More details are discussed later.

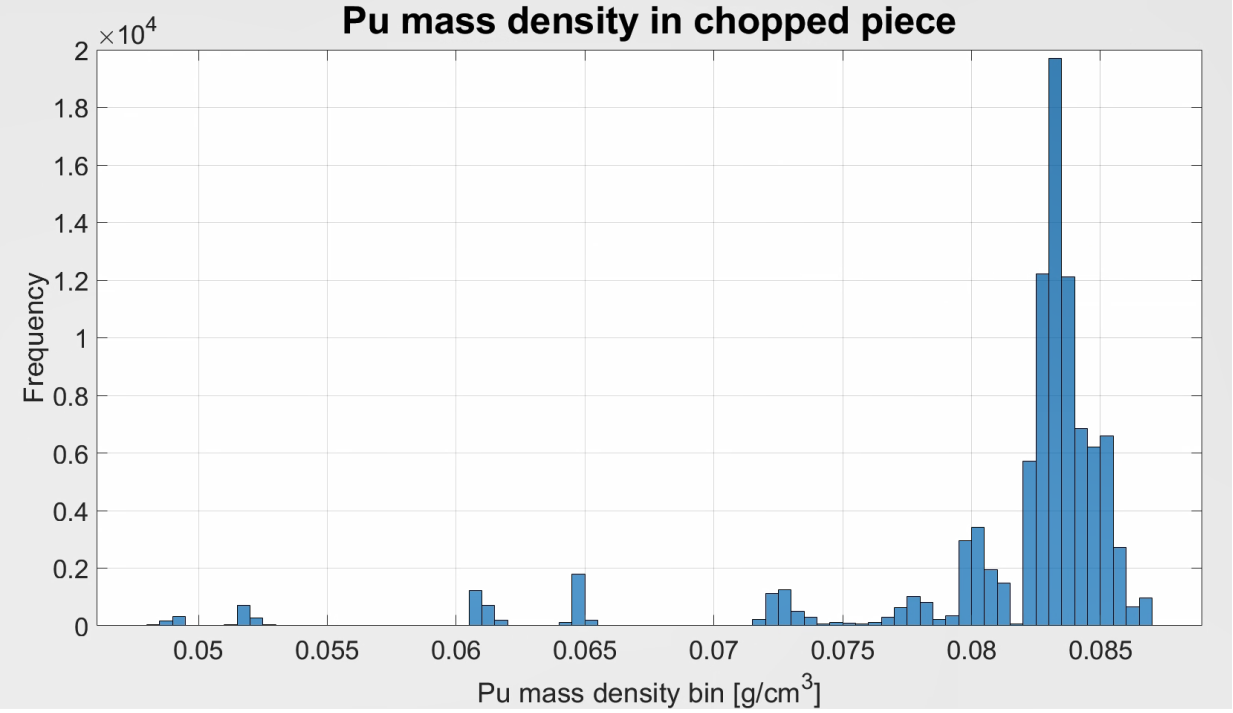

Figure 18. Histogram of Pu Mass Density in Chopped Pieces Processed by the Chopping Process.

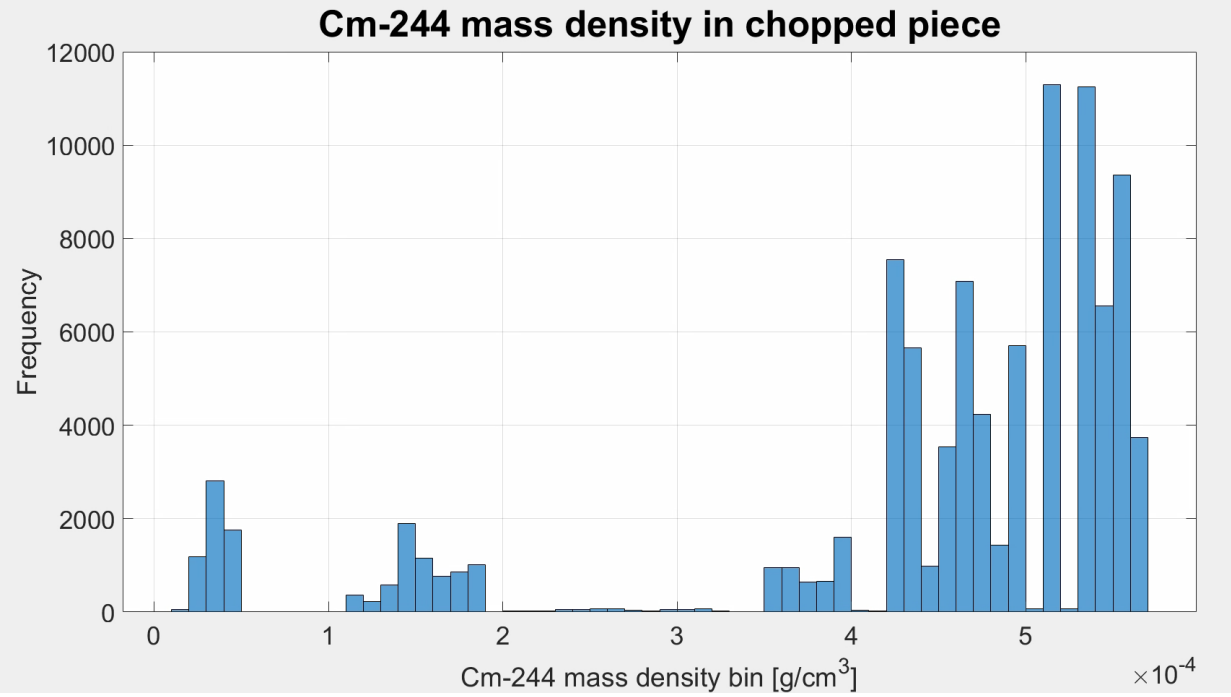

Figure 19. Histogram of ^{244}Cm Mass Density in Chopped Pieces Processed by the Chopping Process.

The expectation values of Pu and ^{244}Cm mass density are plotted in Figures 20 through 29. Each sampling trial is repeated 10,000 times from the population with the sample sizes of 10, 20, 30, 50, and 100. Expectation values seem to follow a normal distribution as the sample size increases. It is expected that if the sample size is reduced, the bell-shaped curve of the figures may be widened or skewed. In other words, the standard deviation increases as sample size is reduced, which is as shown in Figures 30 and 31. This relationship can be explained using

$$\sigma_s = \frac{\sigma_p}{\sqrt{n}} \qquad \text{Eq. 8}$$

Where,

n= sample size

σ_s= sample standard deviation

σ_p= population standard deviation

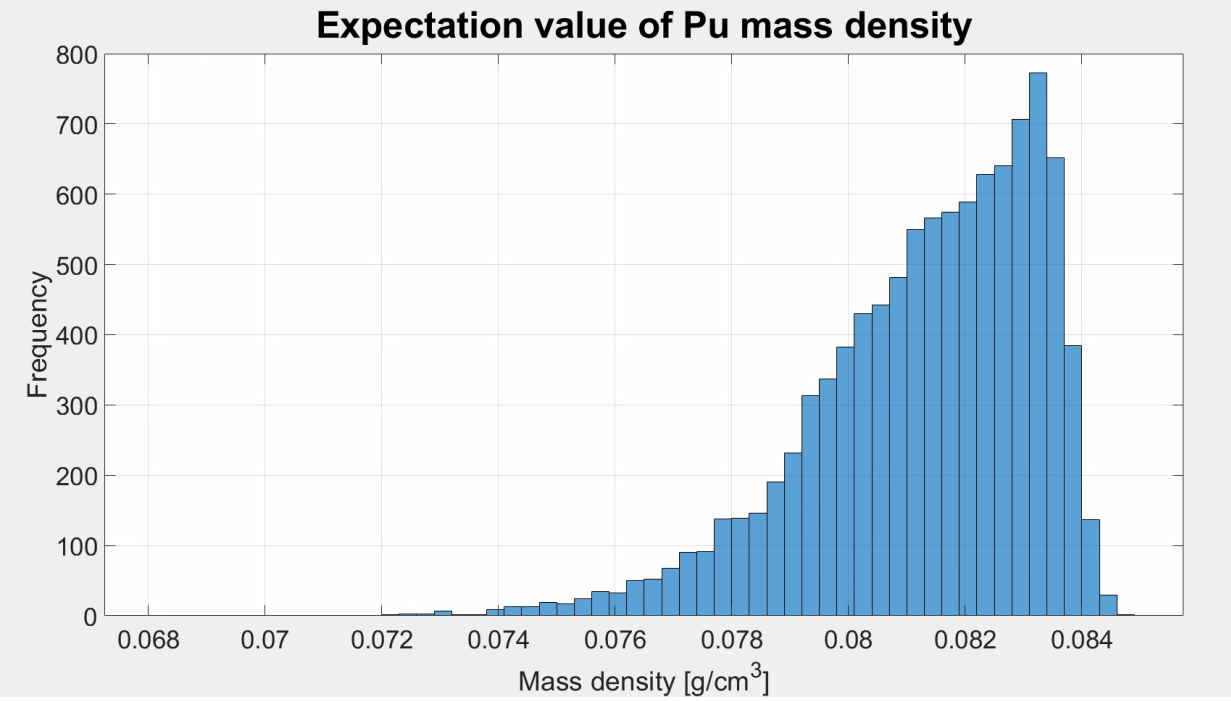

Figure 20. Histogram of the Expected Value for Pu Mass Density. (Sample size = 10)

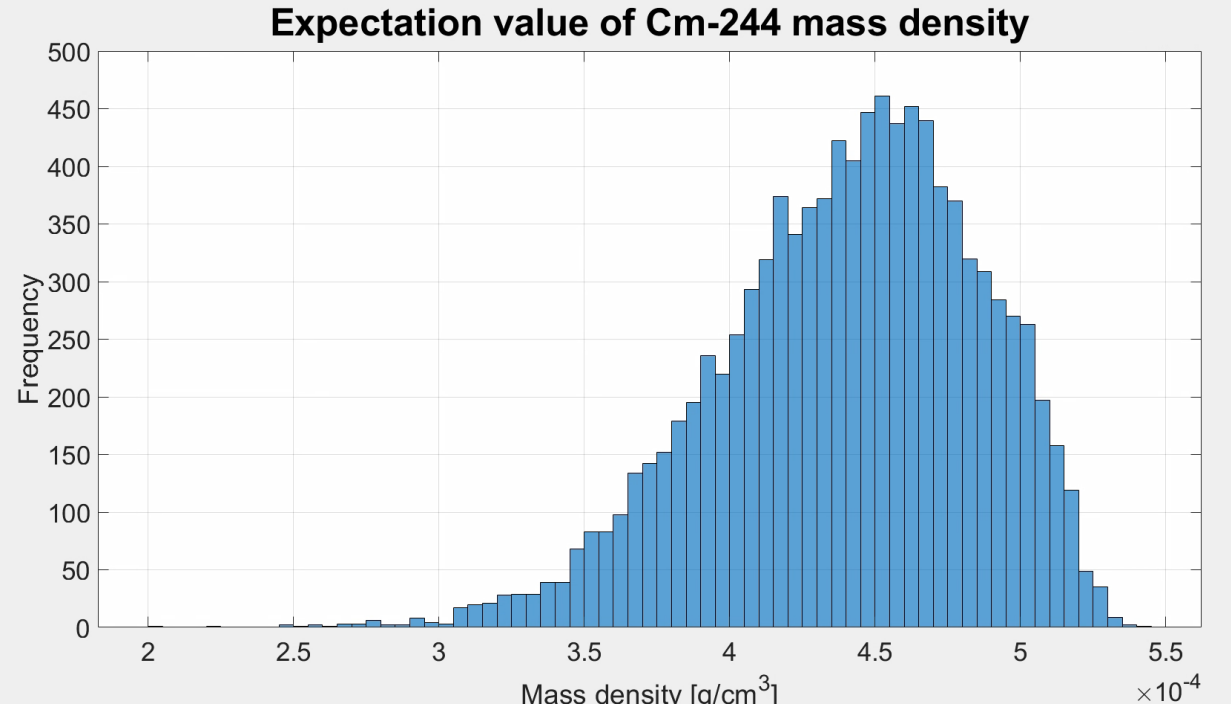

Figure 21. Histogram of the Expected Value for ^{244}Cm Mass Density. (Sample size = 10)

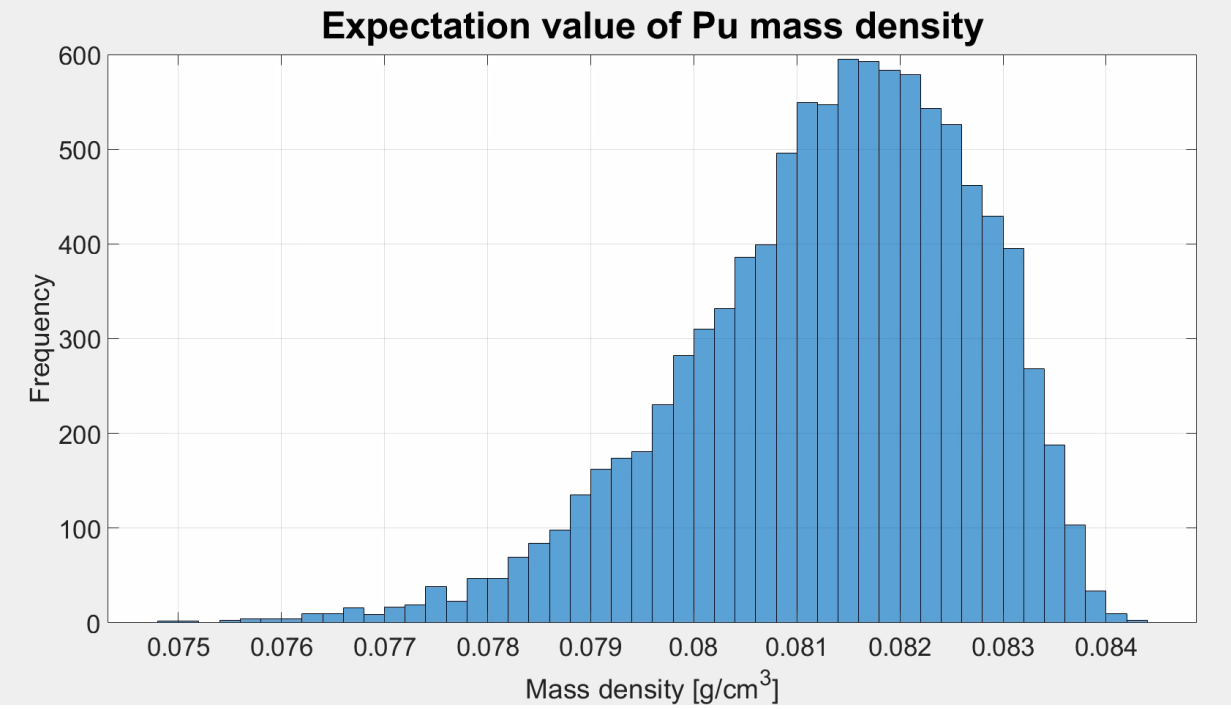

Figure 22. Histogram of the Expected Value for Pu Mass Density. (Sample size = 20)

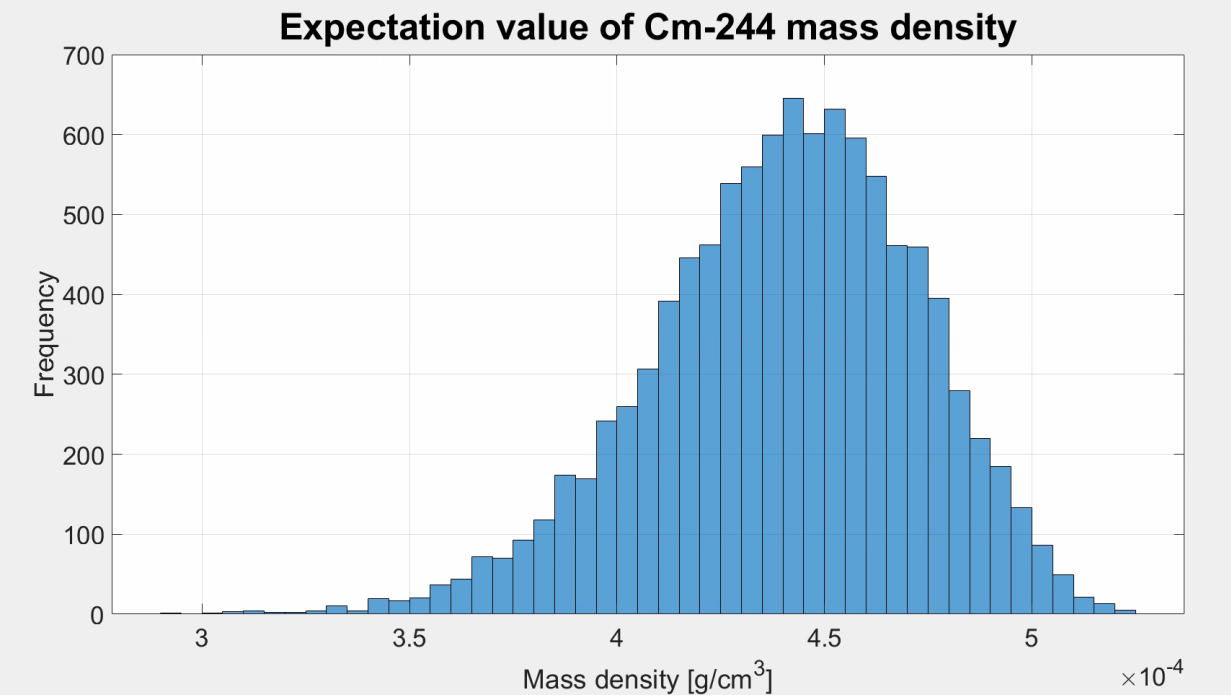

Figure 23. Histogram of the Expected Value for ^{244}Cm Mass Density. (Sample size = 20)

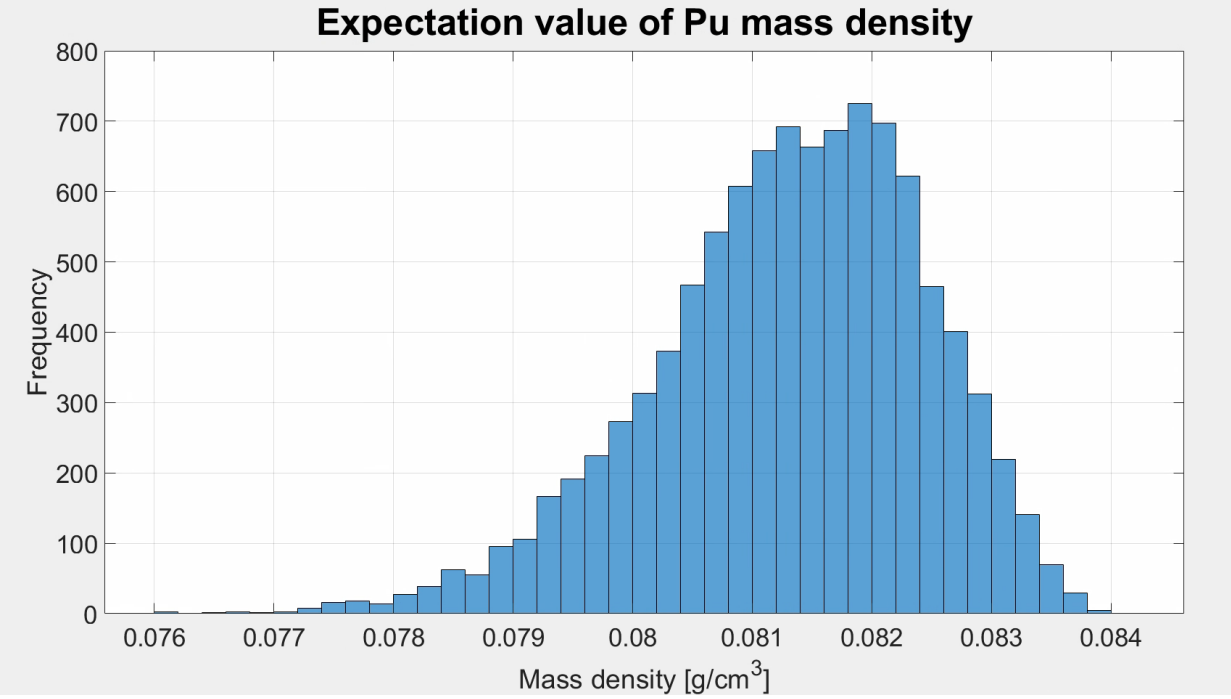

Figure 24. Histogram of the Expected Value for ^{244}Cm Mass Density. (Sample size = 30)

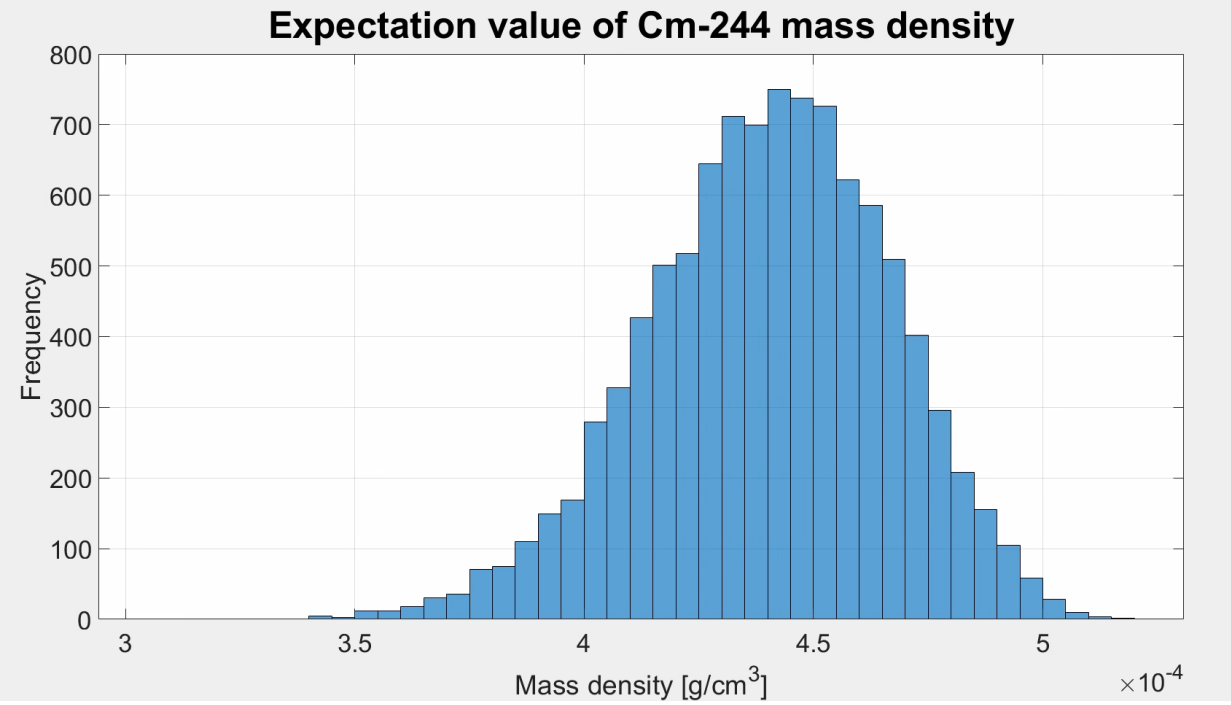

Figure 25. Histogram of the Expected Value for ^{244}Cm Mass Density. (Sample size = 30)

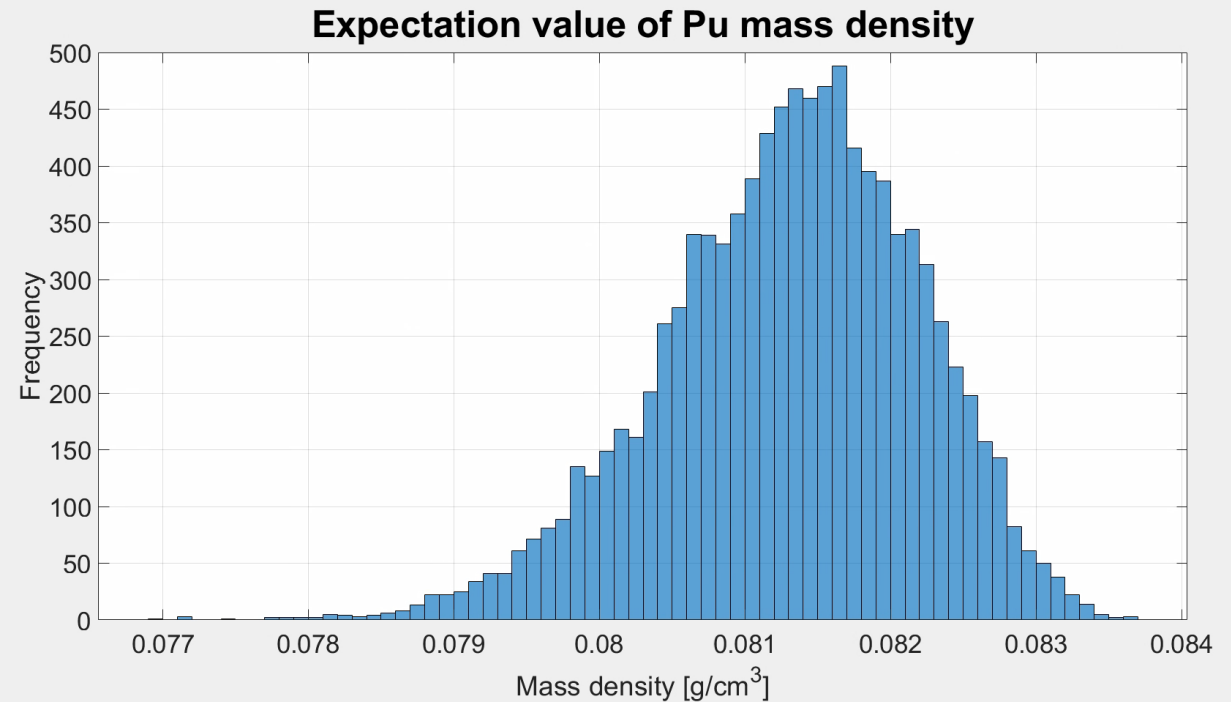

Figure 26. Histogram of the Expected Value for Pu Mass Density. (Sample size = 50)

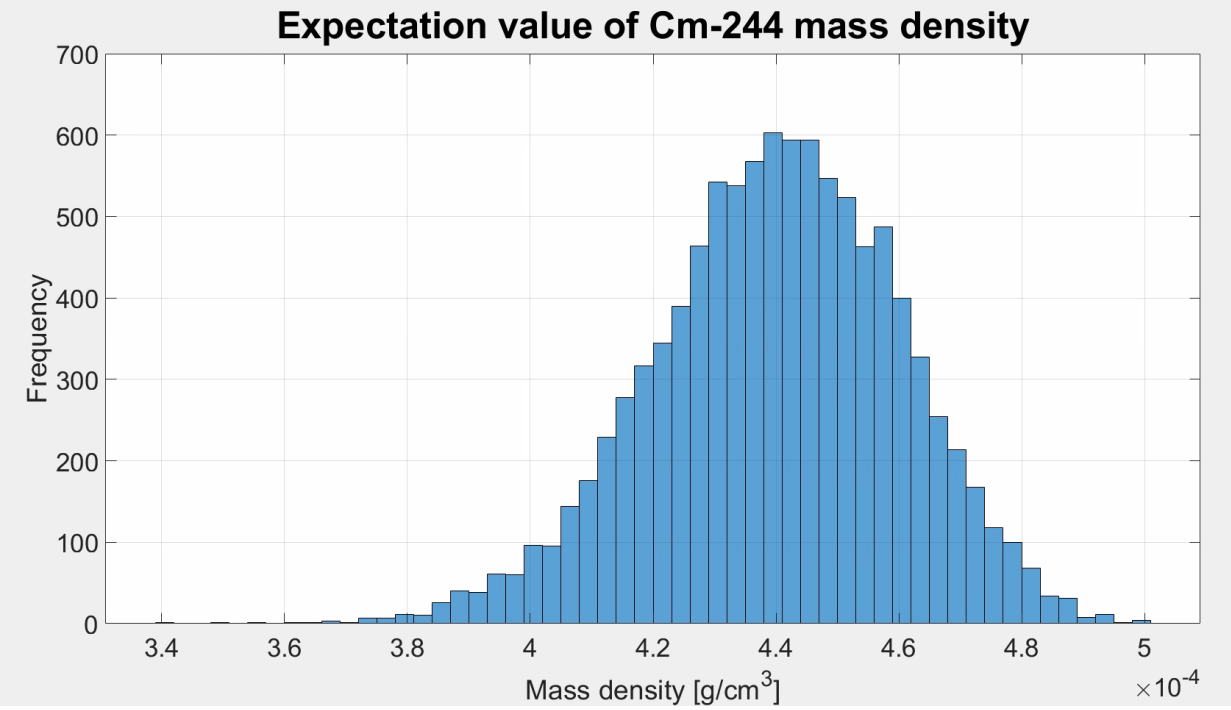

Figure 27. Histogram of the Expected Value for ^{244}Cm Mass Density. (Sample size = 50)

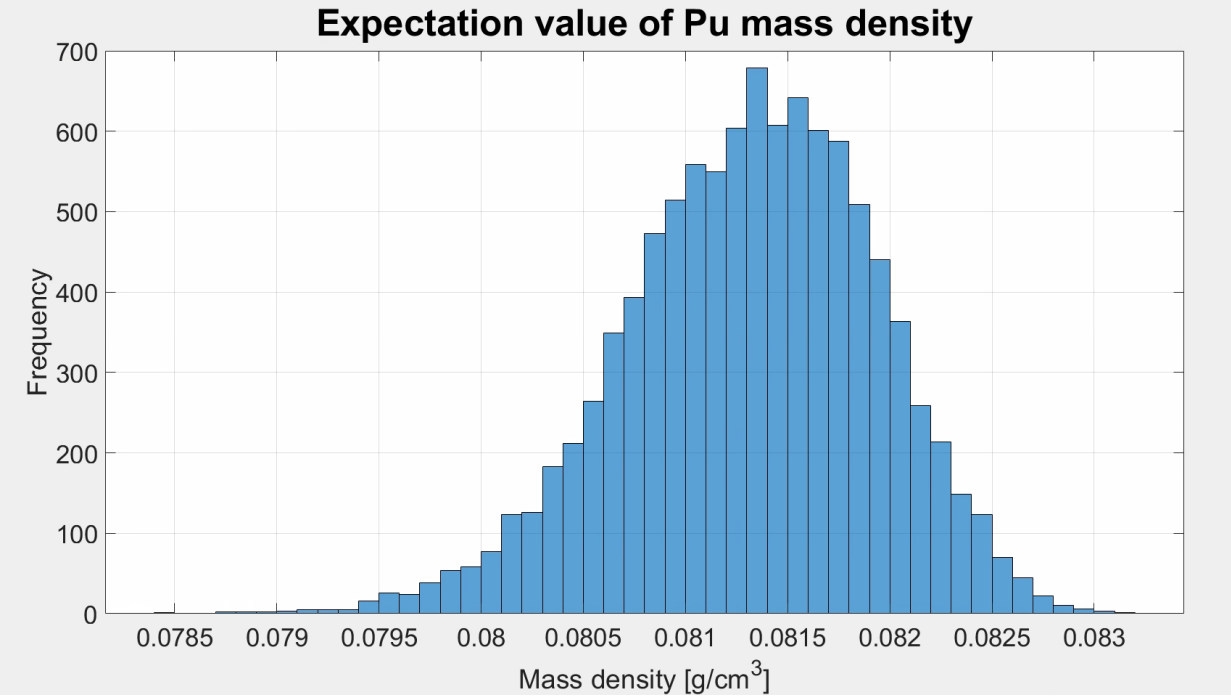

Figure 28. Histogram of the Expected Value for Pu Mass Density. (Sample size = 100)

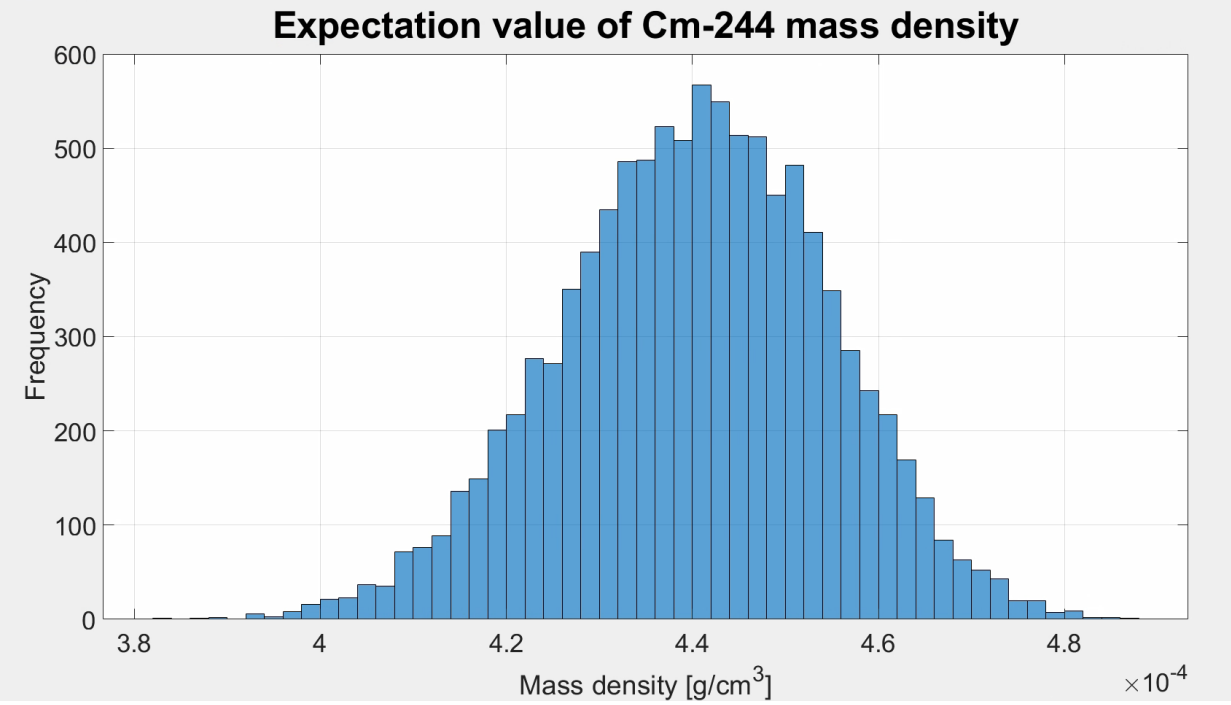

Figure 29. Histogram of the Expected Value for ^{244}Cm Mass Density. (Sample size = 100)

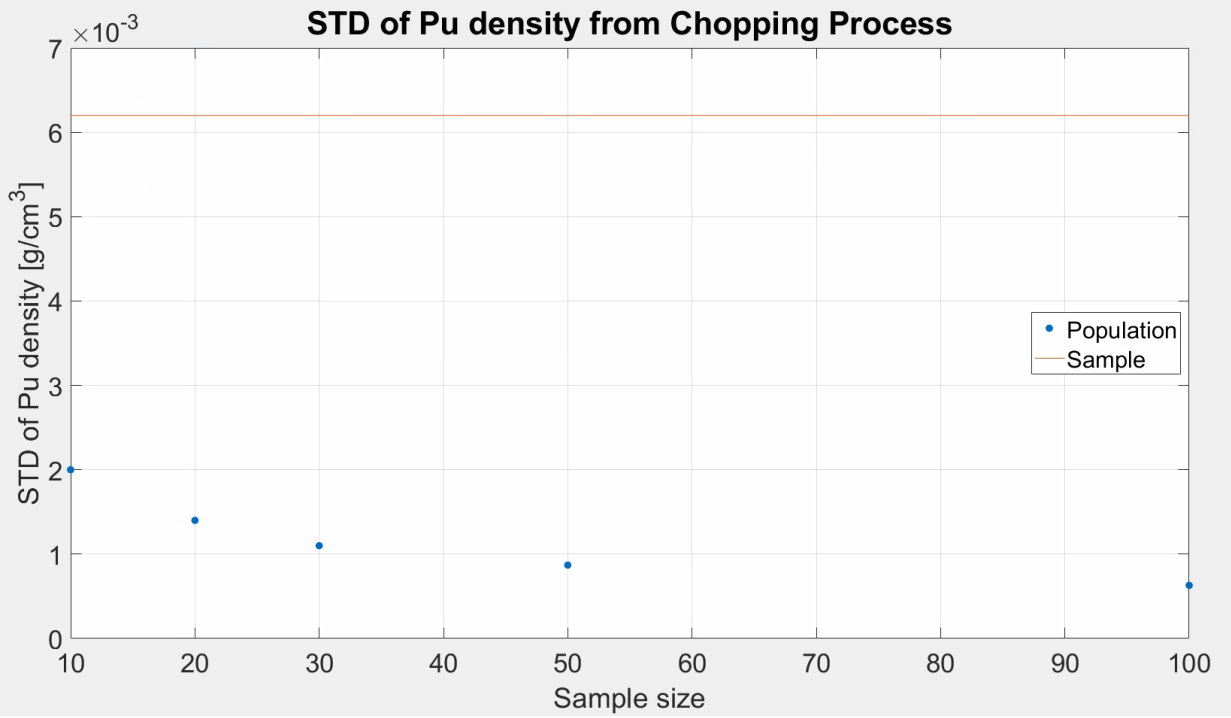

Figure 30. Standard Deviation of Pu Mass Density as a Function of Sample Size.

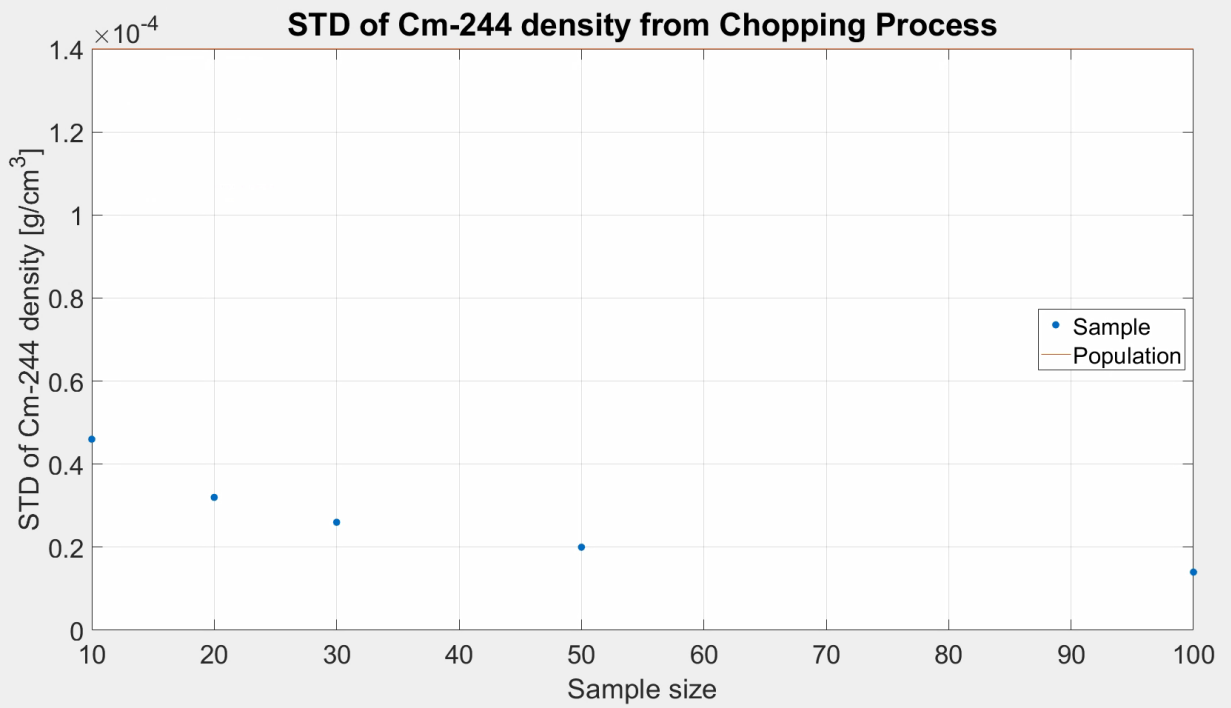

Figure 31. Standard Deviation of ^{244}Cm Mass Density as a Function of Sample Size.

Sampling chopped pieces are repeated 10,000 times with various sample sizes to obtain the uncertainties of the Pu-to-^{244}Cm ratio as listed in Table 7. As the sample size increases, the uncertainty of the Pu-to-^{244}Cm ratio is reduced. However, if only 10 chopped pieces are sampled, the uncertainty of the Pu-to-^{244}Cm ratio is greater than 10% of its value. Moreover, if the uncertainty of the DA method used to obtain the Pu-to-^{244}Cm ratio in the head-end process is considered, it is expected that the propagated uncertainty may increase. The obtained results show that the non-uniformity of the nuclide composition affects NMA in pyroprocess if the KMP is set to measure the Pu-to-^{244}Cm ratio at the end of the chopping process.

Table 7. Mass Densities of Pu and ^{244}Cm, and Pu-to-^{244}Cm Ratio as a Function of the Sample Size with their Uncertainties. ('P-t-C' indicates Pu-to-^{244}Cm ratio. Each sampling cycle is repeated 10,000 times.)

Sample size	Mass density [g/cm^3]				P-t-C	$\sigma_{P\text{-}t\text{-}C}$
	Pu	σ_{Pu}	^{244}Cm	σ_{Cm}		
10	8.13E-02	2.0E-03	4.41E-04	4.6E-05	184.35	19.76
20	8.13E-02	1.4E-03	4.40E-04	3.2E-05	184.77	13.81
30	8.13E-02	1.1E-03	4.40E-04	2.6E-05	184.77	11.20
50	8.13E-02	9.0E-04	4.40E-04	2.0E-05	184.77	8.64
100	8.13E-02	6.0E-04	4.40E-04	1.4E-05	184.77	6.04

Voloxidation Process

The MATLAB code is utilized to simulate the random sampling procedures from voloxidized powders processed by the voloxidation process as shown in Figure 32. As depicted, nuclide compositions, especially Pu and ^{244}Cm, and particle sizes are randomly sampled from previously obtained data. This sampling cycle is repeated until the cumulative volume of the sampled powders reaches the assumed lab spoon's volume. Once this condition is fulfilled, the mean and the standard deviation of the Pu-to-^{244}Cm ratio is calculated.

3 volumes which are 0.05 ml, 0.1 ml, and 0.5 ml are assumed as the lab spoon's volumes. The simulation results are listed in Table 8. Since the simulations are very expensive due to a lot of particles sampled, only one calculation is conducted for each assumed lab spoon's volume. For instance, about 36,000,000 powders are sampled to fill 0.5 ml spoon. The sampled powder volume distribution in the 0.5 ml lab spoon is plotted in Figure 33. The mean values of Pu, ^{244}Cm, and the Pu-to-^{244}Cm ratio are almost the same as those of the chopping process. The uncertainties, however, are much less than those of the chopping process. Especially, if sampling is conducted

using 0.5 ml lab spoon, the uncertainty is 0. In other words, the non-uniformity of nuclide composition does not affect the Pu estimation if the sample for DA is taken from the voloxidation process. By comparing the results from the chopping process and the voloxidation process, it is obvious that the Pu-to-^{244}Cm ratio should be measured at the voloxidation process to minimize the uncertainties.

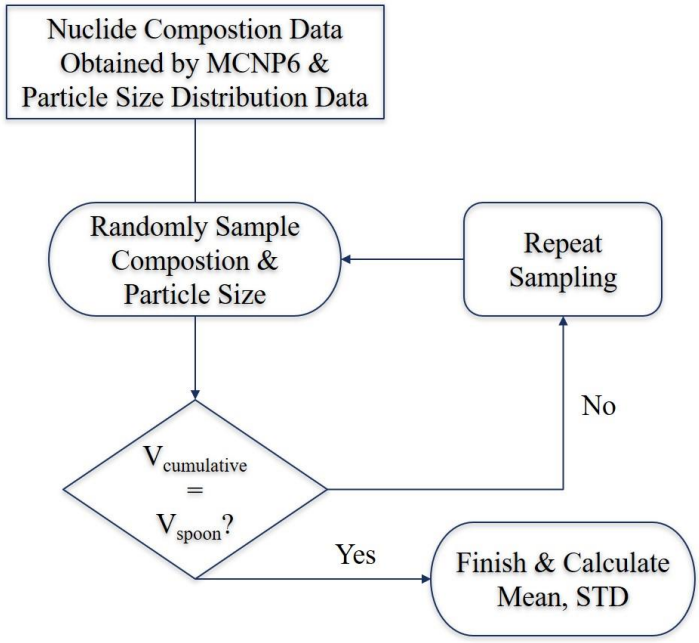

Figure 32. Flow Chart of the MATLAB Simulation Depicting Sampling Scheme from Voloxidation by MATLAB.

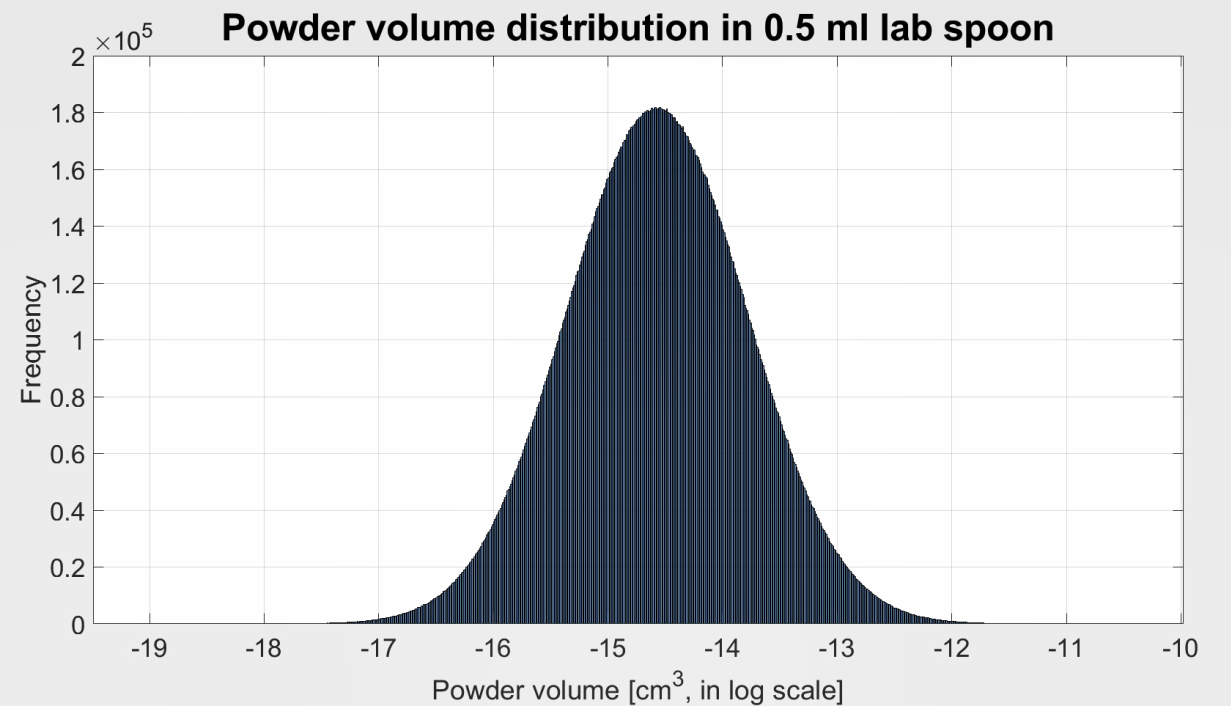

Figure 33. Powder Volume Distribution in 0.5 ml Lab Spoon.

Table 8. Mass Densities of Pu and ^{244}Cm, and Pu-to-^{244}Cm Ratio with Their Uncertainties Depending on Assumed Volume of Lab Spoon. ('P-t-C' indicates the Pu-to-^{244}Cm ratio.)

Volume of lab spoon	Mass density [g/cm^3]				P-t-C	$\sigma_{P\text{-}t\text{-}C}$
	Pu	σ_{Pu}	^{244}Cm	σ_{Cm}		
0.5 ml	8.13E-02	0	4.4E-04	0	184.77	0
0.1 ml	8.13E-02	2.0E-04	4.4E-04	0	184.81	0.68
0.05 ml	8.13E-02	2.0E-04	4.4E-04	0	184.64	0.87

MUF and Sigma-MUF Calculations Considering Detector's Uncertainties

MUF and σ_{MUF} are estimated using previously obtained values and IAEA ITVs of the detection techniques used to measure Pu and ^{244}Cm. In order to investigate practically, ITVs should be considered as well as the uncertainties that are originated from the non-uniformity. The layout

of the assumed MBA for the pyroprocess facility is shown in Figure 34[12]. The chopped fuel and voloxidized powders are assumed as the feed materials to compare. Moreover, the uncertainties of used fuel measurements are also considered.

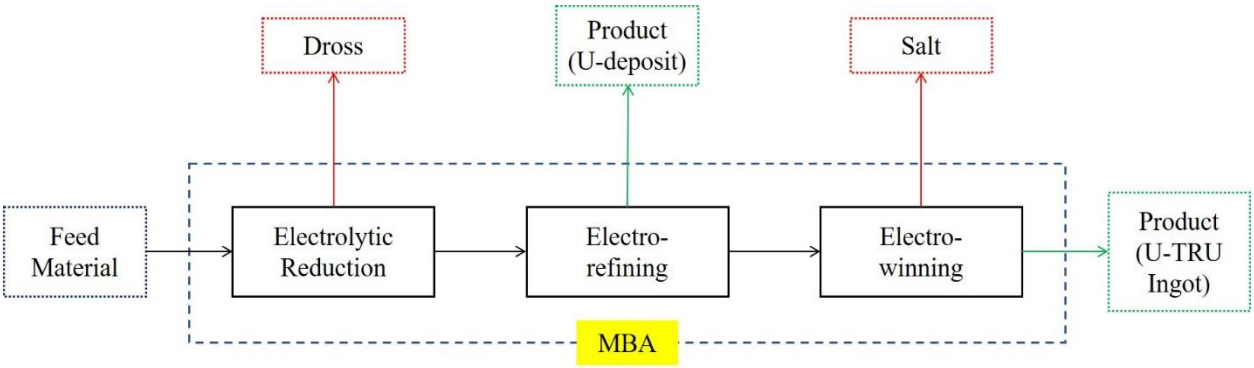

Figure 34. Assumed MBA for the Pyroprocessing Facility. (This MBA is referred from the literature paper published by Woo[12].)

MUF and σ_{MUF} can be calculated using the below Eq. 9 and 9-1.

$$MUF = F - P_D - P_U - P_S - P_{TRU} \quad \text{Eq. 9}$$

$$\sigma_{MUF} = \sqrt{\sigma_F^2 + \sigma_{P_D}^2 + \sigma_{P_U}^2 + \sigma_{P_S}^2 + \sigma_{P_{TRU}}^2} \quad \text{Eq. 9-1}$$

Where,

MUF= MUF for the assumed MBA

F= feed material

P_D= dross from the electrolytic reduction process

P_U= U deposit from the electrorefining process

P_S= salt waste from the electrowinning process

P_{TRU}= TRU ingot from the key-pyroprocess.

Pu-to-^{244}Cm Ratio Estimation in the Feed Materials

The feed material is measured using the DA method and other products are measured using the NDA methods as shown in Table 9. ITVs of those measurements are referred from the reference[25,26].

Table 9. Measurement Techniques and Their Uncertainties.

Material	Method		Random [%]	System [%]	ITV [%]
Feed	DA	IDMS	0.2	0.2	0.28
Dross	NDA	HLNC	10	5	11
U deposit	NDA	HLNC	10	5	11
Salt	NDA	HLNC	10	5	11
TRU	NDA	HLNC	2	1	2.2

If the measurement's uncertainty is considered, the obtained results listed in Tables 7 and 8 are revised as shown in Tables 10 through 12. Applied DA method to measure Pu is Isotope Dilution Mass Spectrometry (IDMS), which has 0.28 % ITV value[26]. Moreover, High Level Neutron Counting (HLNC) is assumed to be used to estimate ^{244}Cm in the feed materials. The ITV value for HLNC is 2.2 %[26]. Tables 10 and 11 show the uncertainties for Pu and ^{244}Cm in chopped pieces and sampled powders from the voloxidation process. As can be seen from Tables 10 and 11, the uncertainties increase since ITV's are additionally added. Because the uncertainties in measurements of Pu and ^{244}Cm increase, the uncertainty of the Pu-to-^{244}Cm ratio also increases as listed in Table 12 for both chopped pieces and voloxidized powders.

Table 10. Calculation Data from the Chopping Process considering Detector's Uncertainty.

Sample size	Mass density [g/cm^3]							
	Pu	σ_{Pu}	σ_{Det}	$\sigma_{T,Pu}$	^{244}Cm	σ_{Cm}	σ_{Det}	$\sigma_{T,Cm}$
10	8.13E-2	2.0E-3	2.0E-4	2.0E-3	4.41E-4	4.6E-5	1.0E-5	4.7E-5
20	8.13E-2	1.4E-3	2.0E-4	1.4E-3	4.40E-4	3.2E-5	1.0E-5	3.3E-5
30	8.13E-2	1.1E-3	2.0E-4	1.1E-3	4.40E-4	2.6E-5	1.0E-5	2.8E-5
50	8.13E-2	9.0E-4	2.0E-4	9.0E-4	4.40E-4	2.0E-5	1.0E-5	2.2E-5
100	8.13E-2	6.0E-4	2.0E-4	6.0E-4	4.40E-4	1.4E-5	1.0E-5	1.7E-5

Table 11. Calculation Data from the Voloxidation Process considering Detector's Uncertainty.

Lab spoon volume	Mass density [g/cm^3]							
	Pu	σ_{Pu}	σ_{Det}	$\sigma_{T,Pu}$	Cm	σ_{Cm}	σ_{Det}	$\sigma_{T,Cm}$
0.5 ml	8.13E-2	0	2.0E-4	2.0E-4	4.40E-4	0	1.0E-5	1.0E-5
0.1 ml	8.13E-2	2.0E-4	2.0E-4	3.0E-4	4.40E-4	1.0E-6	1.0E-5	1.0E-5
0.05 ml	8.13E-2	2.0E-4	2.0E-4	3.0E-4	4.40E-4	2.0E-6	1.0E-5	1.0E-5

Table 12. Uncertainties for Pu-to-^{244}Cm Ratio considering Detector's Uncertainties.

Chopping		
Sample size	P-t-C	$\sigma_{P\text{-}t\text{-}C}$
10	184.35	20.18
20	184.77	14.34
30	184.77	11.87
50	184.77	9.52
100	184.77	7.26
Voloxidation		
Volume	P-t-C	$\sigma_{P\text{-}t\text{-}C}$
0.5 ml	184.77	4.10
0.1 ml	184.81	4.16
0.05 ml	184.64	4.19

Pu Estimation through the Key-pyroprocess

In order to estimate Pu through the key-pyroprocess, the yield and the efficiency of each process are required and is taken from a reference literature[2]. Moreover, no loss during the head-end process is assumed. The production yields for each process are listed in Table 13. Actually, the final product of the pyroprocess is the U-TRU ingot. It is assumed in the reference literature that about 99% of U in used fuel is deposited during the electro-refining process and the remaining 1% of U is mixed with TRUs in the U-TRU ingot.

Table 13. Yields for TRU Elements in the Key-pyroprocess.

Electrolytic reduction		
Product	TRU	99.5 %
Dross	TRU	0.5 %
Electrorefining		
Salt	TRU	99 %
U deposit	TRU	1 %
Electrowinning		
Product	TRU	99 %
Waste	TRU	1 %

In order to calculate MUF and σ_{MUF}, the amount of Pu in dross, U deposit, electrowinning waste, and TRU ingot should be obtained. Because the Pu-to-^{244}Cm ratio already has been determined during the head-end process, the amount of Pu after in the key-pyroprocess can be also measured as described early by using the Pu-to-^{244}Cm ratio method. The Pu estimation for the first process of the key-pyroprocess, which is the electrolytic reduction is listed in Table 14. Eleven percent of ITV for HLNC is assumed as the detector's uncertainty while using to measure ^{244}Cm in the product and dross from the reduction process. After measuring ^{244}Cm, the Pu-to-^{244}Cm ratio is multiplied by the measured ^{244}Cm to estimate Pu. Moreover, the yields mentioned in Table 13 are applied for both product and dross. The product is transferred to the next process which is the electrorefining. The dross is removed from the key-pyroprocess, so it should be considered in calculating MUF. The procedures to estimate Pu from other processes are the same as the method used in the electrolytic reduction process. The results of Pu estimations for the electrorefining and the electrowinning steps are listed in Tables 15 and 16. Eleven percent of ITV for HLNC is applied to the salts and the U deposit for the electrorefining process. This is also used to estimate ^{244}Cm in

the waste of the electrowinning process. In addition, 2.2 % of ITV for HLNC is utilized for the TRU metal which is the final product of the key-pyroprocess.

Table 14. Pu Estimation for the Electrolytic Reduction Process.

Chopping sample size	Product [g/cm^3]				Dross [g/cm^3]			
	^{244}Cm	σ_{Cm}	Pu	σ_{Pu}	^{244}Cm	σ_{Cm}	Pu	σ_{Pu}
10	4.39E-04	4.83E-05	8.09E-02	1.26E-02	2.21E-06	2.43E-07	4.07E-04	6.31E-05
20	4.38E-04	4.82E-05	8.09E-02	1.09E-02	2.20E-06	2.42E-07	4.07E-04	5.47E-05
30	4.38E-04	4.82E-05	8.09E-02	1.03E-02	2.20E-06	2.42E-07	4.07E-04	5.18E-05
50	4.38E-04	4.82E-05	8.09E-02	9.83E-03	2.20E-06	2.42E-07	4.07E-04	4.94E-05
100	4.38E-04	4.82E-05	8.09E-02	9.45E-03	2.20E-06	2.42E-07	4.07E-04	4.75E-05
Voloxi-dation lab spoon volume	^{244}Cm	σ_{Cm}	Pu	σ_{Pu}	^{244}Cm	σ_{Cm}	Pu	σ_{Pu}
0.5 ml	4.38E-04	4.82E-05	8.09E-02	9.08E-03	2.20E-06	2.42E-07	4.07E-04	4.56E-05
0.1 ml	4.38E-04	4.81E-05	8.09E-02	9.08E-03	2.20E-06	2.42E-07	4.07E-04	4.56E-05
0.05 ml	4.38E-04	4.82E-05	8.09E-02	9.09E-03	2.20E-06	2.42E-07	4.07E-04	4.57E-05

Table 15. Pu Estimation for the Electrorefining Process.

Chopping sample size	Salts [g/cm^3]				U deposit [g/cm^3]			
	^{244}Cm	σ_{Cm}	Pu	σ_{Pu}	^{244}Cm	σ_{Cm}	Pu	σ_{Pu}
10	4.34E-04	4.78E-05	8.01E-02	1.24E-02	4.39E-06	4.83E-07	8.09E-04	1.26E-04
20	4.33E-04	4.77E-05	8.01E-02	1.08E-02	4.38E-06	4.82E-07	8.09E-04	1.09E-04
30	4.33E-04	4.77E-05	8.01E-02	1.02E-02	4.38E-06	4.82E-07	8.09E-04	1.03E-04
50	4.33E-04	4.77E-05	8.01E-02	9.73E-03	4.38E-06	4.82E-07	8.09E-04	9.83E-05
100	4.33E-04	4.77E-05	8.01E-02	9.35E-03	4.38E-06	4.82E-07	8.09E-04	9.45E-05
Voloxi-dation lab spoon volume	^{244}Cm	σ_{Cm}	Pu	σ_{Pu}	^{244}Cm	σ_{Cm}	Pu	σ_{Pu}
0.5 ml	4.33E-04	4.77E-05	8.01E-02	8.99E-03	4.38E-06	4.82E-07	8.09E-04	9.08E-05
0.1 ml	4.33E-04	4.77E-05	8.01E-02	8.99E-03	4.38E-06	4.81E-07	8.09E-04	9.08E-05
0.05 ml	4.34E-04	4.77E-05	8.01E-02	8.99E-03	4.38E-06	4.82E-07	8.09E-04	9.09E-05

Table 16. Pu Estimation for the Electrowinning Process.

Chopping sample size	TRU metal [g/cm^3]				Waste [g/cm^3]			
	^{244}Cm	σ_{Cm}	Pu	σ_{Pu}	^{244}Cm	σ_{Cm}	Pu	σ_{Pu}
10	4.30E-04	9.46E-06	7.93E-02	8.85E-03	4.34E-06	4.78E-07	8.01E-04	1.24E-04
20	4.29E-04	9.44E-06	7.93E-02	6.40E-03	4.33E-06	4.77E-07	8.01E-04	1.08E-04
30	4.29E-04	9.44E-06	7.93E-02	5.39E-03	4.33E-06	4.77E-07	8.01E-04	1.02E-04
50	4.29E-04	9.44E-06	7.93E-02	4.44E-03	4.33E-06	4.77E-07	8.01E-04	9.73E-05
100	4.29E-04	9.44E-06	7.93E-02	3.57E-03	4.33E-06	4.77E-07	8.01E-04	9.35E-05
Voloxi-dation lab spoon volume	^{244}Cm	σ_{Cm}	Pu	σ_{Pu}	^{244}Cm	σ_{Cm}	Pu	σ_{Pu}
0.5 ml	4.29E-04	9.44E-06	7.93E-02	2.48E-03	4.33E-06	4.77E-07	8.01E-04	8.99E-05
0.1 ml	4.29E-04	9.44E-06	7.93E-02	2.49E-03	4.33E-06	4.77E-07	8.01E-04	8.99E-05
0.05 ml	4.29E-04	9.45E-06	7.93E-02	2.50E-03	4.34E-06	4.77E-07	8.01E-04	8.99E-05

MUF and Sigma-MUF (σ_{MUF}) Estimation

All values required to estimate MUF and σ_{MUF} for Pu accountancy are obtained as described in the previous section. MUF and σ_{MUF} values for Pu are calculated using Eq. 9 and 9-1 and the obtained values are listed in Table 17. The results in Table 17 are for the one-eighth fuel assembly and these MUF and σ_{MUF} values for the entire fuel assembly is listed in Table 18. The results are converted from the mass density to the mass considering the volume of the fuel assembly.

Table 17. Result for MUF and Sigma-MUF Calculation for One-eighth Fuel Assembly.

Chopping Sample size	MUF [g/cm^3]	σ_{MUF} [g/cm^3]
10	N/A	9.08E-03
20	N/A	6.55E-03
30	N/A	5.50E-03
50	N/A	4.54E-03
100	N/A	3.63E-03
Lab spoon volume	MUF [g/cm^3]	σ_{MUF} [g/cm^3]
0.5 ml	N/A	2.49E-03
0.1 ml	N/A	2.52E-03
0.05 ml	N/A	2.53E-03

Table 18. Result for MUF and Sigma-MUF Calculation for the Entire Fuel Assembly.

Chopping sample size	MUF [g]	σ_{MUF} [g]
10	N/A	4.24E+02
20	N/A	3.06E+02
30	N/A	2.57E+02
50	N/A	2.12E+02
100	N/A	1.69E+02
Lab spoon volume	MUF [g]	σ_{MUF} [g]
0.5 ml	N/A	1.16E+02
0.1 ml	N/A	1.17E+02
0.05 ml	N/A	1.18E+02

According to the first condition of the IAEA's nuclear safeguards criteria, MUF should be less than 8 kg of Pu. The calculated MUF values are small enough to be ignored, so the first condition is met. In addition, MUF should be less than three times σ_{MUF}. This condition is also fulfilled since all MUF values are less than the σ_{MUF} values in all cases. As expected, the σ_{MUF} is the smallest if the voloxidized powders are sampled for the DA method using the 0.5 ml lab spoon in the head-end process to estimate the Pu-to-^{244}Cm ratio. Therefore, the third condition that three times σ_{MUF} should be less than 8 kg of Pu needs to be satisfied as well. The comparisons between the σ_{MUF} and the 1 SQ of Pu which is 8 kg are listed in Table 19. The maximum available throughput is 22 fuel assemblies if the voloxidized powders are selected as the sample to measure the Pu-to-^{244}Cm ratio in the head-end process. If it is assumed that the pyroprocessing facility processes 4 fuel assemblies daily, MBP should be less than 6 days to fulfill the third condition of IAEA's criteria.

Table 19. Three Times Sigma-MUF (σ_{MUF}) and Possible Throughput.

Chopping Sample Size	3-σ_{MUF} [g]	Possible Throughput [No. of Fuel Assemblies]
10	1.27E+03	6
20	9.17E+02	8
30	7.70E+02	10
50	6.36E+02	12
100	5.08E+02	15
Lab spoon volume	3-σ_{MUF} [g]	Possible Throughput [No. of Fuel Assemblies]
0.5 ml	3.49E+02	22
0.1 ml	3.52E+02	22
0.05 ml	3.54E+02	22

CHAPTER IV

SUMMARY AND CONCLUSIONS

Summary

There are several sources of the uncertainty for NMA in the pyroprocessing system, but this study focuses on the effect of the non-uniformity of nuclide compositions in used nuclear fuel assemblies on NMA. In order to investigate this effect, a fuel assembly fuel burnup simulation using MCNP6 is conducted first. Only one-eighth of a PWR fresh fuel assembly is burned because of the fuel assembly symmetry. After the simulation, the results from MCNP6 code is verified by comparing the stochastic uncertainties of MCNP6 to the non-uniformity of Pu. The needed condition was that the MCNP's stochastic uncertainties should be less than the Pu non-uniformity because this study investigates the effect of the non-uniformity on Pu NMA.

The axial and radial distributions of nuclide composition, especially Pu and ^{244}Cm, are then investigated by analyzing obtained data from MCNP6 simulations. The Pu and ^{244}Cm mass densities varied depending on the axial and radial location in the used fuel assembly. Those distributions are caused by the temperature variation in the reactor core, neutron flux variations and the rim-effect of the fuel rod.

Then, those obtained nuclide composition data are modified properly to depict feed materials of the pyroprocessing facility such as the chopped pieces and the voloxidized powders. In order to depict the head-end process including the chopping and the voloxidation processes, a MATLAB code script is developed. For the chopping process, the obtained composition data from MCNP6 code in all fuel rods are axially divided as the used fuel assemblies are chopped in the chopping process. The Pu and ^{244}Cm composition in chopped pieces are then collected with the

various sample sizes of the chopped pieces. The expectation value and the standard deviation for the Pu-to-^{244}Cm ratio of chopped pieces are estimated.

In addition, the voloxidation process powders are sampled using MATLAB code script. The powder size distribution was referred from literature. By using the powder size distribution, the number of powders needed to fill the assumed lab spoon is decided. Then, each powder in the lab spoon is matched with the composition data obtained by MCNP6. After that, the Pu-to-^{244}Cm ratio and the standard deviation of the ratio in the lab spoon are evaluated. The uncertainty of the Pu-to-^{244}Cm ratio of the voloxidized powders is found to be much smaller than that of the chopped pieces.

Then, the MUF and the sigma-MUF through the key-pyroprocess are calculated using the obtained Pu-to-^{244}Cm ratio values and ITVs. The MUF and the sigma-MUF (σ_{MUF}) values are smaller if the sampling to determine the Pu-to-^{244}Cm ratio was conducted at the voloxidation process rather than the chopping process. Finally, the available throughput for the pyroprocessing facility considering the IAEA's criteria was evaluated.

Conclusions

This study was conducted to investigate the effect of the non-uniformity on the Pu-to-^{244}Cm ratio method of NMA in pyroprocessing. As described in chapter III, nuclide non-uniformity exists in used nuclear fuel. To be specific, the axial and radial non-uniformities of nuclide compositions are studied. The variation of the moderator's temperature, the rim-effect, and the various location for each fuel rod in the fuel assembly caused the non-uniformity in nuclide composition, specifically for Pu and Cm. The non-uniformity of Pu and ^{244}Cm, however, did not affect the NMA in pyroprocessing if samples to estimate the Pu-to-^{244}Cm ratio in the head-end process were taken

from the voloxidized powders, which were products of the voloxidation process. Finally, the available throughput for the assumed pyroprocessing facility and the MBP to meet the IAEA's standard are evaluated using the obtained values and ITVs.

In summary, the contributions of this project can be concluded as follows. (1) Development of the MCNP6 code input to obtain the nuclide composition in the used fuel assembly. (2) Development of a methodology to estimate the Pu-to-^{244}Cm ratio from both chopped pieces and voloxidized powders of pyroprocess. (3) Analysis of the effect of the non-uniformity of the nuclide composition on the Pu estimation in pyroprocessing. (4) MUF and the sigma-MUF estimation by using the obtained Pu-to-^{244}Cm ratio and ITVs in the assumed MBA.

Although it is proven that the non-uniformity does not influence the Pu-to-^{244}Cm ratio method in pyroprocessing, there are other weak points for the Pu-to-^{244}Cm ratio method. For instance, the replacement of ^{244}Cm in used nuclear fuel can be a possible diversion scenario. This is because the Pu-to-^{244}Cm ratio method is using the fact that ^{244}Cm is a dominant spontaneous fission source in used nuclear fuel. Therefore, if the TRU ingot which contains Pu and ^{244}Cm is replaced with other spontaneous fission neutron sources such as ^{252}Cf, the Pu in the TRU ingot can be diverted. Therefore, when designing safeguards approaches for the pyroprocessing facility, this aspect should be considered carefully.

REFERENCES

1. Lee, H. *et al.* Pyroprocessing Technology Development at KAERI. *Nucl. Eng. Technol.* **43,** 317–328 (2011).

2. Yoo, J. H., Seo, C. S., Kim, E. H. & Lee, H. S. A Conceptual Study of Pyroprocessing for Recovering Actinides from Spent Oxide Fuels. *Nucl. Eng. Technol.* **40,** 581–592 (2008).

3. Seo, H. *et al.* Optimization of Hybrid-type Instrumentation for Pu Accountancy of U/TRU Ingot in Pyroprocessing. *Appl. Radiat. Isot.* **108,** 16–23 (2016).

4. IAEA. IAEA Safeguards Technical Manual. **3,** (1982).

5. Miura, N. & Menlove, H. O. The Use of Curium Neutrons to Verify Plutonium in Spent Fuel and Reprocessing Wastes. (1994).

6. Pelowitz, D. B. *et al.* MCNP6 User's Manual. (2013).

7. Dahlheimer, J. A. *et al.* The Westinghouse Pressurized Water Reactor Nuclear Power Plant. (1984).

8. IAEA. IAEA Safeguards Glossary. (2003).

9. Ahn, S. K., Shin, H. S. & Kim, H. D. Safeguardability Analysis for an Engineering Scale Pyroprocess Facility. *J. Nucl. Sci. Technol.* **49,** 632–639 (2012).

10. Lee, T. H., Kim, Y. S., Kwon, T. J., Shin, H. S. & Kim, H. D. Determination of the Plutonium Mass and Curium Ratio of Spent Fuel Assemblies for Input Nuclear Material Accountancy of Pyroprocessing, and Analysis of Their Errors. *Nucl. Technol.* **179,** 196–204 (2012).

11. Woo, S. M., Boo, H. J., Chirayath, S. S. & Jeong, K. H. Investigations on Detecting Potential Nuclear Material Diversion from a Pyroprocessing Facility Investigations on Detecting Potential Nuclear Material Diversion from a Pyroprocessing Facility. *Nucl. Technol.* **205,** 464–473 (2019).

12. Woo, S. M., Chirayath, S. S. & Fratoni, M. Nuclide Composition Non-uniformity in Used Nuclear Fuel for Considerations in Pyroprocessing Safeguards. *Nucl. Eng. Technol.* **50,** 1120–1130 (2018).

13. Song, K. W., Kim, K. S., Kim, Y. M. & Jung, Y. H. Sintering of Mixed UO_2 and U_3O_8 Powder Compacts. *J. Nucl. Mater.* **277,** 123–129 (2000).

14. IAEA. Safeguards Techniques and Equipment. (2003).

15. Duderstadt, J. J. & Hamilton, L. J. Nuclear Reactor Analysis. (1976).

16. Jarque, C. M. & Bera, A. K. A Test for Normality of Observations and Regression Residuals. *Int. Stat. Rev.* **55,** 163–172 (1987).

17. Ensslin, N. The Origin of Neutron Radiation. 337–356 (1991).

18. Ensslin, N. Principles of Neutron Coincidence Counting. Passive Nondestructive Assay Manual (PANDA) (1991).

19. Ensslin, N. *et al.* Passive Neutron Multiplicity Counting. 6–20 (2007).

20. El-gammal, W. A., Mostafa, A. G. & Ebied, M. On the Mathematical Calibration of the Active Well Neutron Coincidence Counter (AWCC). *Am. J. Phys. Appl.* **3,** 121–130 (2015).

21. Lee, Y. G., Cha, H. R., Kim, H. D., Hong, J. S. & Kang, H. Y. Development of DUPIC Safeguards Neutron Counter. (1999).

22. Akie, H., Sato, I., Suzuki, M., Serizawa, H. & Arai, Y. Simple Formula to Evaluate Helium Production Amount in Fast Reactor MA-Containing MOX Fuel and Its Accuracy. *J. Nucl. Sci. Technol.* **50,** 107–121 (2013).

23. Woo, S. M. Development of A Methodology to Evaluate Material Accountability in Pyroprocess. (2017).

24. Matzke, H. On the Rim Effect in High Burnup UO_2 LWR Fuels. *J. Nucl. Mater.* **189,** 141–148 (1992).

25. Chang, H. L., Gao, F. X., Ko, W. I. & Kim, H. D. Evaluation of Sigma-MUF (Material Unaccounted For) for the Conceptually Designed Korea Advanced Pyroprocess Facility. *J. Korean Phys. Soc.* **59,** 1418–1421 (2011).

26. Zhao, K. *et al.* International Target Values 2010 for Measurement Uncertainties in Safeguarding Nuclear Materials. (2012).

APPENDIX A

MCNP6 INPUT DECK

1/8 Fuel Assembly

The below cell card for fuel-1 is repeated to fuel-12 to make 12 universes.
Therefore, the cell cards for fuel 2 to fuel 12 are omitted.

```
C    -----------fuel-1----------------------------------
1100    9999 -0.7426       -101              u=1 imp:n=1              $below plenum
1101    0           -4     101 -102          u=1 imp:n=1              $upper plenum
1102    9998 -6.3902  4 -5  101 -102          u=1 imp:n=1              $upper plenum
1104  1  -10.339  -2  102  -103  vol=2.2378   u=1 imp:n=1   $R1-Ax1
1105  2  -10.339  -2  103  -104  vol=6.6441   u=1 imp:n=1   $R1-Ax2
1106  3  -10.339  -2  104  -105  vol=10.8500  u=1 imp:n=1   $R1-Ax3
1107  4  -10.339  -2  105  -107  vol=32.8785  u=1 imp:n=1   $R1-Ax4
1108  5  -10.339  -2  107  -110  vol=189.3408 u=1 imp:n=1   $R1-Ax5
1109  6  -10.339  -2  110  -112  vol=32.8785  u=1 imp:n=1   $R1-Ax6
1110  7  -10.339  -2  112  -113  vol=10.8500  u=1 imp:n=1   $R1-Ax7
1111  8  -10.339  -2  113  -114  vol=6.6441   u=1 imp:n=1   $R1-Ax8
1112  9  -10.339  -2  114  -115  vol=2.2378   u=1 imp:n=1   $R1-Ax9
1113  10  -10.339  2  -3  102  -103  vol=1.1195   u=1 imp:n=1   $R2-Ax1
1114  11  -10.339  2  -3  103  -104  vol=3.3239   u=1 imp:n=1   $R2-Ax2
1115  12  -10.339  2  -3  104  -105  vol=5.4280   u=1 imp:n=1   $R2-Ax3
1116  13  -10.339  2  -3  105  -107  vol=16.4485  u=1 imp:n=1   $R2-Ax4
1117  14  -10.339  2  -3  107  -110  vol=94.7236  u=1 imp:n=1   $R2-Ax5
1118  15  -10.339  2  -3  110  -112  vol=16.4485  u=1 imp:n=1   $R2-Ax6
1119  16  -10.339  2  -3  112  -113  vol=5.4280   u=1 imp:n=1   $R2-Ax7
1120  17  -10.339  2  -3  113  -114  vol=3.3239   u=1 imp:n=1   $R2-Ax8
1121  18  -10.339  2  -3  114  -115  vol=1.1195   u=1 imp:n=1   $R2-Ax9
1143    0           3 -4  102 -115          u=1 imp:n=1 tmp=5.1702E-08
1144    9998  -6.3902  4 -5  102 -115          u=1 imp:n=1 tmp=5.1702E-08
1145    0           -4     115 -116          u=1 imp:n=1              $Vaccum upper plenum
1146    9998  -6.3902  4 -5  115 -116          u=1 imp:n=1              $Cladding for upper plenum
1147    9999  -0.6642  5     115 -116          u=1 imp:n=1
1148    9999  -0.6642       116               u=1 imp:n=1
1149    9999  -0.7426  5     101 -102          u=1 imp:n=1              $Inlet 1st
1150    9999  -0.7426  5     102 -200          u=1 imp:n=1              $      2
1151    9999  -0.7423  5     200 -201          u=1 imp:n=1              $      3
1152    9999  -0.7419  5     201 -202          u=1 imp:n=1              $      4
1153    9999  -0.7411  5     202 -203          u=1 imp:n=1              $      5
1154    9999  -0.7402  5     203 -204          u=1 imp:n=1              $      6
1155    9999  -0.7390  5     204 -205          u=1 imp:n=1              $      7
1156    9999  -0.7376  5     205 -206          u=1 imp:n=1              $      8
1157    9999  -0.7360  5     206 -207          u=1 imp:n=1              $      9
1158    9999  -0.7342  5     207 -208          u=1 imp:n=1              $      10
```

```
1159  9999  -0.7321  5    208 -209        u=1 imp:n=1          $    11
1160  9999  -0.7299  5    209 -210        u=1 imp:n=1          $    12
1161  9999  -0.7275  5    210 -211        u=1 imp:n=1          $    13
1162  9999  -0.7249  5    211 -212        u=1 imp:n=1          $    14
1163  9999  -0.7222  5    212 -213        u=1 imp:n=1          $    15
1164  9999  -0.7193  5    213 -214        u=1 imp:n=1          $    16
1165  9999  -0.7163  5    214 -215        u=1 imp:n=1          $    17
1166  9999  -0.7132  5    215 -216        u=1 imp:n=1          $    18
1167  9999  -0.7100  5    216 -217        u=1 imp:n=1          $    19
1168  9999  -0.7067  5    217 -218        u=1 imp:n=1          $    20
1169  9999  -0.7034  5    218 -219        u=1 imp:n=1          $    21
1170  9999  -0.7000  5    219 -220        u=1 imp:n=1          $    22
1171  9999  -0.6966  5    220 -221        u=1 imp:n=1          $    23
1172  9999  -0.6933  5    221 -222        u=1 imp:n=1          $    24
1173  9999  -0.6900  5    222 -223        u=1 imp:n=1          $    25
1174  9999  -0.6867  5    223 -224        u=1 imp:n=1          $    26
1175  9999  -0.6836  5    224 -225        u=1 imp:n=1          $    27
1176  9999  -0.6806  5    225 -226        u=1 imp:n=1          $    28
1177  9999  -0.6778  5    226 -227        u=1 imp:n=1          $    29
1178  9999  -0.6752  5    227 -228        u=1 imp:n=1          $    30
1179  9999  -0.6728  5    228 -229        u=1 imp:n=1          $    31
1180  9999  -0.6706  5    229 -230        u=1 imp:n=1          $    32
1181  9999  -0.6687  5    230 -231        u=1 imp:n=1          $    33
1182  9999  -0.6672  5    231 -232        u=1 imp:n=1          $    34
1183  9999  -0.6659  5    232 -233        u=1 imp:n=1          $    35
1184  9999  -0.6650  5    233 -234        u=1 imp:n=1          $    36
1185  9999  -0.6644  5    234 -235        u=1 imp:n=1          $    37
1186  9999  -0.6642  5    235 -115        u=1 imp:n=1          $    38
C    ----------guide tubes----------
301  9999  -0.7426      -101       u=99   imp:n=1 $Inlet 1st water region
302  9999  -0.7426  -4   101 -102  u=99   imp:n=1 $     2
303  9999  -0.7426  -4   102 -200  u=99   imp:n=1 $     2
304  9999  -0.7423  -4   200 -201  u=99   imp:n=1 $     3
305  9999  -0.7419  -4   201 -202  u=99   imp:n=1 $     4
306  9999  -0.7411  -4   202 -203  u=99   imp:n=1 $     5
307  9999  -0.7402  -4   203 -204  u=99   imp:n=1 $     6
308  9999  -0.7390  -4   204 -205  u=99   imp:n=1 $     7
309  9999  -0.7376  -4   205 -206  u=99   imp:n=1 $     8
310  9999  -0.7360  -4   206 -207  u=99   imp:n=1 $     9
311  9999  -0.7342  -4   207 -208  u=99   imp:n=1 $     10
312  9999  -0.7321  -4   208 -209  u=99   imp:n=1 $     11
313  9999  -0.7299  -4   209 -210  u=99   imp:n=1 $     12
314  9999  -0.7275  -4   210 -211  u=99   imp:n=1 $     13
315  9999  -0.7249  -4   211 -212  u=99   imp:n=1 $     14
316  9999  -0.7222  -4   212 -213  u=99   imp:n=1 $     15
317  9999  -0.7193  -4   213 -214  u=99   imp:n=1 $     16
```

```
318  9999  -0.7163  -4    214 -215  u=99   imp:n=1 $     17
319  9999  -0.7132  -4    215 -216  u=99   imp:n=1 $     18
320  9999  -0.7100  -4    216 -217  u=99   imp:n=1 $     19
321  9999  -0.7067  -4    217 -218  u=99   imp:n=1 $     20
322  9999  -0.7034  -4    218 -219  u=99   imp:n=1 $     21
323  9999  -0.7000  -4    219 -220  u=99   imp:n=1 $     22
324  9999  -0.6966  -4    220 -221  u=99   imp:n=1 $     23
325  9999  -0.6933  -4    221 -222  u=99   imp:n=1 $     24
326  9999  -0.6900  -4    222 -223  u=99   imp:n=1 $     25
327  9999  -0.6867  -4    223 -224  u=99   imp:n=1 $     26
328  9999  -0.6836  -4    224 -225  u=99   imp:n=1 $     27
329  9999  -0.6806  -4    225 -226  u=99   imp:n=1 $     28
330  9999  -0.6778  -4    226 -227  u=99   imp:n=1 $     29
331  9999  -0.6752  -4    227 -228  u=99   imp:n=1 $     30
332  9999  -0.6728  -4    228 -229  u=99   imp:n=1 $     31
333  9999  -0.6706  -4    229 -230  u=99   imp:n=1 $     32
334  9999  -0.6687  -4    230 -231  u=99   imp:n=1 $     33
335  9999  -0.6672  -4    231 -232  u=99   imp:n=1 $     34
336  9999  -0.6659  -4    232 -233  u=99   imp:n=1 $     35
337  9999  -0.6650  -4    233 -234  u=99   imp:n=1 $     36
338  9999  -0.6644  -4    234 -235  u=99   imp:n=1 $     37
339  9999  -0.6642  -4    235 -116  u=99   imp:n=1 $     38
340  9998  -6.3902   4 -5 101 -116  u=99   imp:n=1 $     $tube cladding
341  9999  -0.7426   5    101 -102  u=99   imp:n=1 $     2
343  9999  -0.7426   5    102 -200  u=99   imp:n=1 $     2
344  9999  -0.7423   5    200 -201  u=99   imp:n=1 $     3
345  9999  -0.7419   5    201 -202  u=99   imp:n=1 $     4
346  9999  -0.7411   5    202 -203  u=99   imp:n=1 $     5
347  9999  -0.7402   5    203 -204  u=99   imp:n=1 $     6
348  9999  -0.7390   5    204 -205  u=99   imp:n=1 $     7
349  9999  -0.7376   5    205 -206  u=99   imp:n=1 $     8
350  9999  -0.7360   5    206 -207  u=99   imp:n=1 $     9
351  9999  -0.7342   5    207 -208  u=99   imp:n=1 $     10
352  9999  -0.7321   5    208 -209  u=99   imp:n=1 $     11
353  9999  -0.7299   5    209 -210  u=99   imp:n=1 $     12
354  9999  -0.7275   5    210 -211  u=99   imp:n=1 $     13
355  9999  -0.7249   5    211 -212  u=99   imp:n=1 $     14
356  9999  -0.7222   5    212 -213  u=99   imp:n=1 $     15
357  9999  -0.7193   5    213 -214  u=99   imp:n=1 $     16
358  9999  -0.7163   5    214 -215  u=99   imp:n=1 $     17
359  9999  -0.7132   5    215 -216  u=99   imp:n=1 $     18
360  9999  -0.7100   5    216 -217  u=99   imp:n=1 $     19
361  9999  -0.7067   5    217 -218  u=99   imp:n=1 $     20
362  9999  -0.7034   5    218 -219  u=99   imp:n=1 $     21
363  9999  -0.7000   5    219 -220  u=99   imp:n=1 $     22
364  9999  -0.6966   5    220 -221  u=99   imp:n=1 $     23
```

```
365  9999  -0.6933   5    221 -222  u=99   imp:n=1 $     24
366  9999  -0.6900   5    222 -223  u=99   imp:n=1 $     25
367  9999  -0.6867   5    223 -224  u=99   imp:n=1 $     26
368  9999  -0.6836   5    224 -225  u=99   imp:n=1 $     27
369  9999  -0.6806   5    225 -226  u=99   imp:n=1 $     28
370  9999  -0.6778   5    226 -227  u=99   imp:n=1 $     29
371  9999  -0.6752   5    227 -228  u=99   imp:n=1 $     30
372  9999  -0.6728   5    228 -229  u=99   imp:n=1 $     31
373  9999  -0.6706   5    229 -230  u=99   imp:n=1 $     32
374  9999  -0.6687   5    230 -231  u=99   imp:n=1 $     33
375  9999  -0.6672   5    231 -232  u=99   imp:n=1 $     34
376  9999  -0.6659   5    232 -233  u=99   imp:n=1 $     35
377  9999  -0.6650   5    233 -234  u=99   imp:n=1 $     36
378  9999  -0.6644   5    234 -235  u=99   imp:n=1 $     37
379  9999  -0.6642   5    235 -116  u=99   imp:n=1 $     38
380  9999  -0.6642        116       u=99   imp:n=1 $
C    ----------------Assembly lattice----------------------
1    0  6 -7  8 -9 lat=1 fill=-8:8 -8:8 0:0
     12 1  1  1  1  1  1  1  1  1  1  1  1  1  1  1  12
     12 12 1  1  1  1  1  1  1  1  1  1  1  1  1  12 12
     12 11 10 1  1  1  1  1  1  1  1  1  1  1  10 11 12
     11 10 9  99 1  1  1  1  1  1  1  1  1  99 9  10 11
     10 9  8  7  6  1  1  1  1  1  1  1  6  7  8  9  10
     9  8  99 6  5  99 1  1  1  1  1  99 5  6  99 8  9
     8  7  6  5  4  3  2  1  1  1  2  3  4  5  6  7  8
     7  6  5  4  3  2  1  1  1  1  1  2  3  4  5  6  7
     6  5  99 3  2  99 1  1  99 1  1  99 2  3  99 5  6
     3  3  3  3  3  3  3  3  2  2  2  2  2  2  2  2  2
     3  3  3  3  3  3  3  3  2  2  2  2  2  2  2  2  2
     3  3  3  3  3  3  3  3  2  2  2  2  2  2  2  2  2
     3  3  3  3  3  3  3  3  2  2  2  2  2  2  2  2  2
     3  3  3  3  3  3  3  3  2  2  2  2  2  2  2  2  2
     3  3  3  3  3  3  3  3  2  2  2  2  2  2  2  2  2
     3  3  3  3  3  3  3  3  2  2  2  2  2  2  2  2  2
     3  3  3  3  3  3  3  3  2  2  2  2  2  2  2  2  2  u=100 imp:n=1
2    0        -999 10 -99 100 -117     fill=100 imp:n=1
999  0          999:-10:99:-100:117              imp:n=0

c surface card
1       cz     0.2264       $ Inner fuel in radial
2       cz     0.3202       $ Middle fuel in radial
3       cz     0.3922       $ Outer fuel in radial
4       cz     0.40005      $ Feul clad IR
5       cz     0.457        $ Feul clad OR
6       PX    -0.63         $ fuel rod pitch : 1.26 cm
7       PX     0.63         $ pitch
```

```
8     PY   -0.63       $ fuel rod pitch : 1.26 cm
9     PY    0.63
100    pz  -238.9        $below reflector
101    pz  -188.9        $below plenum
102    pz  -182.9        $fuel pin down height
103    pz  -180.121       $ 1st mesh
104    pz  -171.870       $ 2
105    pz  -158.396       $ 3
106    pz  -140.110       $ 4
107    pz  -117.566       $ 5
108    pz  -91.45        $ 6
109    pz   91.45        $ 7
110    pz   117.566       $ 8
111    pz   140.110       $ 9
112    pz   158.396       $10
113    pz   171.870       $11
114    pz   180.121       $12
115    pz   182.9        $13
116    pz   202.9        $Upper plenum
117    pz   252.9        $upper reflector
c
200    pz -172.9    $ 1st water region
201    pz -162.9    $ 2nd
202    pz -152.9    $ 3
203    pz -142.9    $ 4
204    pz -132.9    $ 5
205    pz -122.9    $ 6
206    pz -112.9    $ 7
207    pz -102.9    $ 8
208    pz -92.9     $ 9
209    pz -82.9     $ 10
210    pz -72.9     $ 11
211    pz -62.9     $ 12
212    pz -52.9     $ 13
213    pz -42.9     $ 14
214    pz -32.9     $ 15
215    pz -22.9     $ 16
216    pz -12.9     $ 17
217    pz -2.9      $ 18
218    pz 7.1       $ 19
219    pz 17.1      $ 20
220    pz 27.1      $ 21
221    pz 37.1      $ 22
222    pz 47.1      $ 23
223    pz 57.1      $ 24
224    pz 67.1      $ 25
```

```
225     pz 77.1       $ 26
226     pz 87.1       $ 27
227     pz 97.1       $ 28
228     pz 107.1      $ 29
229     pz 117.1      $ 30
230     pz 127.1      $ 31
231     pz 137.1      $ 32
232     pz 147.1      $ 33
233     pz 157.1      $ 34
234     pz 167.1      $ 35
235     pz 177.1      $ 36
c Assembly
*999    px 10.71 $10.71
*10     py 0.0
*99     p -1 1 0 0

c data card
mode n
kcode 25000 1.3 25 500
sdef pos= 0 0 0 rad=d1 axs= 0 0 1 erg=d3 par=1 ccc=2
si1 0 15.1426 $=sqrt(2*10.71^2)
si2 182.9
sp3 -3
mphys
burn   time= 0.3 0.3 0.4 1 2 5 21 30 30 30 30 30 30 30 30 30
           30 30 30 30 30 30 30 30 30 30
           30 30 30 30 30 30 30 30 30 30
           30 30 26 1825
      pfrac= 1  1  1  1  1  1  1  1  1  1  1  1  1  1  1  1
           1  1  1  1  1  1  1  1  1  1
           1  1  1  1  1  1  1  1  1  1
           1  1  1  0
       power= 2.20875 $ =17.67/8   $ MWth
        mat= 1 2 3 4 5 6 7 8 9 10
           11 12 13 14 15 16 17 18 19 20
           21 22 23 24 25 26 27 28 29 30
           31 32 33 34 35 36 37 38 39 40
           41 42 43 44 45 46 47 48 49 50
           51 52 53 54 55 56 57 58 59 60
           61 62 63 64 65 66 67 68 69 70
           71 72 73 74 75 76 77 78 79 80
           81 82 83 84 85 86 87 88 89 90
           91 92 93 94 95 96 97 98 99 100
           101 102 103 104 105 106 107 108 109 110
           111 112 113 114 115 116 117 118 119 120
           121 122 123 124 125 126 127 128 129 130
```

131 132 133 134 135 136 137 138 139 140
141 142 143 144 145 146 147 148 149 150
151 152 153 154 155 156 157 158 159 160
161 162 163 164 165 166 167 168 169 170
171 172 173 174 175 176 177 178 179 180
181 182 183 184 185 186 187 188 189 190
191 192 193 194 195 196 197 198 199 200
201 202 203 204 205 206 207 208 209 210
211 212 213 214 215 216

The below matvol should include all material volume used. Therefore, the volumes for 216 materials should be inserted. The volumes for material 2 to 216 are omitted.

matvol=2.237799041
AFMIN=1.0e-20
bopt= 1 -4 1 $Q-value, tier1, order oupt inventory based on increasing

The m2 to m216 are omitted because they are the same as m1. Those are material properties for fuel rods for all materials.

```
m1      8016.82c  2.0  92235.82c 0.033  92238.82c 0.967 96244.82c 1E-36
m9998  40090.81c 5.01944E-01 40091.81c 1.09462E-01 $ ZIRCALOY at 600K
      40092.81c 1.67315E-01
      40094.81c 1.69558E-01 40096.81c 2.73167E-02
      50112.81c 1.18836E-04 50114.81c 7.96322E-05 50115.81c 4.41040E-05
      50116.81c 1.78008E-03 50117.81c 9.40884E-04 50118.81c 2.96722E-03
      50119.81c 1.05114E-03 50120.81c 3.99263E-03 50122.81c 5.67226E-04
      50122.81c 7.09339E-04
      26054.81c 2.16063E-04 26056.81c 3.35887E-03 26057.81c 7.69039E-05
      26058.81c 1.02539E-05
      24050.81c 9.49456E-05 24052.81c 1.83095E-03 24053.81c 2.07591E-04
      24054.81c 5.16793E-05
      8016.81c  5.39867E-03 6000.81c  9.08126E-04
m9999  1001.81c  2.0          $H2O at 600K
      8016.81c  1.0
mt9999 LWTR.16t             $ 600K S(alpha,Beta) treatment
f4:n
```

APPENDIX B

VERIFICATION OF MCNP CALCULATION RESULT

Universe	1		2		3		4		5		6		7		8		9		10		11		12	
Mesh	Inner	Outer	Inner	Outer	Inner	Outer	Inner	Outer	Inner	Outer	Inner	Outer	Inner	Outer	Inner	Outer	Inner	Outer	Inner	Outer	Inner	Outer	Inner	Outer
Axial 1	0.0232	0.0154	0.0184	0.0123	0.0232	0.0155	0.0183	0.0120	0.0326	0.0220	0.0374	0.0250	0.0278	0.0186	0.0283	0.0187	0.0282	0.0190	0.0238	0.0158	0.0190	0.0126	0.0287	0.0193
Difference	0.0074	0.0067	0.0061	0.0054	0.0076	0.0068	0.0065	0.0059	0.0106	0.0095	0.0125	0.0106	0.0097	0.0086	0.0095	0.0086	0.0099	0.0082	0.0083	0.0074	0.0070	0.0062	0.0110	0.0094
R	0.3172	0.4327	0.3322	0.4417	0.3280	0.4357	0.3526	0.4887	0.3255	0.4321	0.3340	0.4226	0.3491	0.4640	0.3363	0.4599	0.3512	0.4325	0.3504	0.4686	0.3669	0.4968	0.3844	0.4856
S	0.0186	0.0260	0.0186	0.0289	0.0170	0.0288	0.0195	0.0299	0.0141	0.0212	0.0133	0.0221	0.0138	0.0277	0.0153	0.0271	0.0158	0.0252	0.0189	0.0266	0.0197	0.0314	0.0175	0.0289
Axial 2	0.0306	0.0221	0.0245	0.0178	0.0308	0.0223	0.0248	0.0179	0.0432	0.0314	0.0499	0.0356	0.0375	0.0272	0.0378	0.0273	0.0381	0.0273	0.0321	0.0232	0.0260	0.0188	0.0397	0.0287
Dif	0.0018	0.0014	0.0013	0.0010	0.0016	0.0013	0.0012	0.0008	0.0025	0.0017	0.0028	0.0025	0.0023	0.0017	0.0021	0.0021	0.0025	0.0023	0.0022	0.0016	0.0020	0.0014	0.0028	0.0023
Dif	0.0074	0.0067	0.0061	0.0054	0.0076	0.0068	0.0065	0.0059	0.0106	0.0095	0.0125	0.0106	0.0097	0.0086	0.0095	0.0086	0.0099	0.0082	0.0083	0.0074	0.0070	0.0062	0.0110	0.0094
R	0.0605	0.0633	0.0530	0.0541	0.0532	0.0601	0.0483	0.0460	0.0585	0.0544	0.0558	0.0705	0.0621	0.0613	0.0567	0.0783	0.0653	0.0858	0.0701	0.0682	0.0775	0.0754	0.0710	0.0804
R	0.2408	0.3020	0.2494	0.3064	0.2470	0.3035	0.2607	0.3283	0.2456	0.3017	0.2504	0.2971	0.2587	0.3169	0.2516	0.3150	0.2599	0.3019	0.2595	0.3191	0.2684	0.3319	0.2777	0.3269
S	0.0113	0.0171	0.0117	0.0181	0.0102	0.0166	0.0117	0.0194	0.0089	0.0138	0.0084	0.0130	0.0099	0.0154	0.0095	0.0157	0.0098	0.0154	0.0101	0.0174	0.0118	0.0188	0.0106	0.0159
Axial 3	0.0324	0.0235	0.0258	0.0187	0.0324	0.0236	0.0260	0.0187	0.0457	0.0332	0.0527	0.0381	0.0399	0.0288	0.0399	0.0294	0.0406	0.0296	0.0343	0.0248	0.0280	0.0202	0.0426	0.0310
Dif	0.0013	0.0012	0.0009	0.0009	0.0011	0.0012	0.0008	0.0007	0.0015	0.0014	0.0019	0.0017	0.0012	0.0012	0.0011	0.0015	0.0013	0.0014	0.0010	0.0009	0.0009	0.0008	0.0011	0.0011
Dif	0.0018	0.0014	0.0013	0.0010	0.0016	0.0013	0.0012	0.0008	0.0025	0.0017	0.0028	0.0025	0.0023	0.0017	0.0021	0.0021	0.0025	0.0023	0.0022	0.0016	0.0020	0.0014	0.0028	0.0023
R	0.0416	0.0499	0.0357	0.0481	0.0350	0.0513	0.0306	0.0371	0.0324	0.0422	0.0369	0.0438	0.0308	0.0427	0.0274	0.0497	0.0332	0.0462	0.0288	0.0349	0.0316	0.0391	0.0248	0.0360
R	0.0570	0.0595	0.0504	0.0514	0.0505	0.0567	0.0461	0.0440	0.0552	0.0516	0.0529	0.0659	0.0585	0.0578	0.0537	0.0726	0.0613	0.0790	0.0655	0.0638	0.0719	0.0701	0.0663	0.0744
S	0.0076	0.0117	0.0079	0.0132	0.0070	0.0112	0.0081	0.0128	0.0062	0.0098	0.0058	0.0090	0.0066	0.0105	0.0066	0.0105	0.0070	0.0108	0.0078	0.0115	0.0084	0.0132	0.0074	0.0112
Axial 4	0.0311	0.0223	0.0249	0.0178	0.0313	0.0224	0.0252	0.0180	0.0442	0.0318	0.0508	0.0365	0.0386	0.0276	0.0388	0.0279	0.0392	0.0282	0.0333	0.0239	0.0271	0.0195	0.0415	0.0299
Dif	0.0012	0.0007	0.0009	0.0007	0.0011	0.0008	0.0009	0.0006	0.0015	0.0012	0.0020	0.0015	0.0014	0.0012	0.0014	0.0012	0.0015	0.0011	0.0013	0.0009	0.0010	0.0008	0.0016	0.0012
Dif	0.0013	0.0012	0.0009	0.0009	0.0011	0.0012	0.0008	0.0007	0.0015	0.0014	0.0019	0.0017	0.0012	0.0012	0.0011	0.0015	0.0013	0.0014	0.0010	0.0009	0.0009	0.0008	0.0011	0.0011
R	0.0378	0.0335	0.0348	0.0373	0.0336	0.0367	0.0340	0.0353	0.0346	0.0389	0.0397	0.0401	0.0364	0.0426	0.0373	0.0419	0.0392	0.0377	0.0382	0.0387	0.0383	0.0399	0.0391	0.0387
R	0.0434	0.0525	0.0370	0.0506	0.0363	0.0541	0.0315	0.0386	0.0335	0.0441	0.0384	0.0458	0.0317	0.0446	0.0282	0.0523	0.0343	0.0484	0.0296	0.0362	0.0326	0.0407	0.0254	0.0374
S	0.0040	0.0060	0.0042	0.0065	0.0037	0.0059	0.0041	0.0067	0.0032	0.0050	0.0030	0.0047	0.0034	0.0054	0.0035	0.0055	0.0035	0.0054	0.0039	0.0060	0.0043	0.0068	0.0038	0.0059
Axial 5	0.0323	0.0231	0.0258	0.0185	0.0323	0.0232	0.0261	0.0187	0.0458	0.0330	0.0528	0.0379	0.0400	0.0288	0.0403	0.0291	0.0408	0.0293	0.0346	0.0248	0.0281	0.0202	0.0431	0.0310
Dif	0.0022	0.0017	0.0019	0.0015	0.0022	0.0018	0.0019	0.0015	0.0032	0.0024	0.0037	0.0029	0.0029	0.0022	0.0029	0.0023	0.0029	0.0023	0.0024	0.0019	0.0020	0.0015	0.0032	0.0024
Dif	0.0012	0.0007	0.0009	0.0007	0.0011	0.0008	0.0009	0.0006	0.0015	0.0012	0.0020	0.0015	0.0014	0.0012	0.0014	0.0012	0.0015	0.0011	0.0013	0.0009	0.0010	0.0008	0.0016	0.0012
R	0.0692	0.0752	0.0721	0.0827	0.0690	0.0775	0.0732	0.0805	0.0703	0.0741	0.0707	0.0753	0.0712	0.0774	0.0713	0.0786	0.0712	0.0789	0.0695	0.0756	0.0720	0.0752	0.0738	0.0776
R	0.0364	0.0324	0.0336	0.0360	0.0325	0.0354	0.0329	0.0341	0.0334	0.0374	0.0382	0.0386	0.0351	0.0409	0.0359	0.0402	0.0377	0.0363	0.0368	0.0372	0.0369	0.0384	0.0376	0.0373
S	0.0017	0.0026	0.0018	0.0028	0.0016	0.0025	0.0017	0.0028	0.0013	0.0021	0.0012	0.0020	0.0014	0.0023	0.0015	0.0023	0.0015	0.0023	0.0016	0.0025	0.0018	0.0029	0.0016	0.0024
Axial 6	0.0345	0.0248	0.0276	0.0200	0.0346	0.0250	0.0280	0.0202	0.0490	0.0354	0.0565	0.0408	0.0429	0.0310	0.0432	0.0314	0.0437	0.0316	0.0370	0.0267	0.0302	0.0218	0.0463	0.0334
Dif	0.0008	0.0009	0.0009	0.0006	0.0011	0.0011	0.0007	0.0006	0.0013	0.0015	0.0016	0.0015	0.0010	0.0011	0.0011	0.0010	0.0010	0.0008	0.0009	0.0009	0.0005	0.0007	0.0006	0.0006
Dif	0.0022	0.0017	0.0019	0.0015	0.0022	0.0018	0.0019	0.0015	0.0032	0.0024	0.0037	0.0029	0.0029	0.0022	0.0029	0.0023	0.0029	0.0023	0.0024	0.0019	0.0020	0.0015	0.0032	0.0024
R	0.0240	0.0349	0.0314	0.0302	0.0322	0.0428	0.0258	0.0281	0.0275	0.0428	0.0285	0.0359	0.0243	0.0348	0.0246	0.0321	0.0220	0.0263	0.0256	0.0334	0.0172	0.0324	0.0120	0.0194
R	0.0647	0.0699	0.0673	0.0764	0.0646	0.0719	0.0682	0.0745	0.0656	0.0690	0.0661	0.0700	0.0665	0.0718	0.0665	0.0729	0.0665	0.0731	0.0650	0.0703	0.0672	0.0700	0.0687	0.0720
S	0.0041	0.0062	0.0043	0.0067	0.0038	0.0060	0.0041	0.0066	0.0033	0.0050	0.0031	0.0048	0.0035	0.0054	0.0035	0.0054	0.0036	0.0055	0.0040	0.0062	0.0044	0.0070	0.0039	0.0058
Axial 7	0.0353	0.0257	0.0285	0.0206	0.0357	0.0261	0.0287	0.0207	0.0503	0.0369	0.0581	0.0422	0.0439	0.0321	0.0442	0.0324	0.0446	0.0324	0.0380	0.0276	0.0307	0.0225	0.0469	0.0341
Dif	0.0023	0.0018	0.0021	0.0016	0.0026	0.0021	0.0023	0.0019	0.0039	0.0032	0.0048	0.0037	0.0035	0.0027	0.0037	0.0030	0.0039	0.0029	0.0035	0.0030	0.0030	0.0025	0.0048	0.0035
Dif	0.0008	0.0009	0.0009	0.0006	0.0011	0.0011	0.0007	0.0006	0.0013	0.0015	0.0016	0.0015	0.0010	0.0011	0.0011	0.0010	0.0010	0.0008	0.0009	0.0009	0.0005	0.0007	0.0006	0.0006
R	0.0637	0.0683	0.0729	0.0796	0.0737	0.0805	0.0800	0.0902	0.0774	0.0855	0.0820	0.0866	0.0804	0.0834	0.0841	0.0941	0.0879	0.0895	0.0913	0.1102	0.0977	0.1101	0.1029	0.1024
R	0.0234	0.0337	0.0305	0.0293	0.0312	0.0410	0.0251	0.0273	0.0267	0.0410	0.0277	0.0346	0.0237	0.0336	0.0240	0.0311	0.0215	0.0257	0.0250	0.0324	0.0169	0.0314	0.0118	0.0190
S	0.0077	0.0118	0.0080	0.0127	0.0073	0.0113	0.0080	0.0128	0.0063	0.0097	0.0058	0.0092	0.0070	0.0106	0.0066	0.0105	0.0067	0.0108	0.0075	0.0117	0.0086	0.0129	0.0075	0.0112
Axial 8	0.0331	0.0239	0.0264	0.0190	0.0331	0.0240	0.0264	0.0189	0.0464	0.0338	0.0534	0.0386	0.0404	0.0294	0.0405	0.0293	0.0407	0.0295	0.0345	0.0246	0.0277	0.0200	0.0421	0.0306
Dif	0.0091	0.0081	0.0074	0.0063	0.0092	0.0082	0.0071	0.0060	0.0129	0.0115	0.0149	0.0130	0.0113	0.0095	0.0111	0.0097	0.0115	0.0099	0.0101	0.0083	0.0081	0.0069	0.0123	0.0107
Dif	0.0023	0.0018	0.0021	0.0016	0.0026	0.0021	0.0023	0.0019	0.0039	0.0032	0.0048	0.0037	0.0035	0.0027	0.0037	0.0030	0.0039	0.0029	0.0035	0.0030	0.0030	0.0025	0.0048	0.0035
R	0.2762	0.3369	0.2816	0.3330	0.2797	0.3406	0.2683	0.3166	0.2773	0.3399	0.2785	0.3360	0.2802	0.3230	0.2746	0.3290	0.2819	0.3363	0.2915	0.3398	0.2910	0.3434	0.2932	0.3504
R	0.0681	0.0733	0.0786	0.0864	0.0795	0.0876	0.0869	0.0991	0.0839	0.0935	0.0893	0.0948	0.0874	0.0910	0.0918	0.1038	0.0964	0.0983	0.1005	0.1238	0.1082	0.1237	0.1147	0.1141
S	0.0115	0.0170	0.0115	0.0186	0.0103	0.0172	0.0119	0.0185	0.0091	0.0145	0.0085	0.0134	0.0093	0.0157	0.0097	0.0153	0.0097	0.0166	0.0116	0.0177	0.0116	0.0186	0.0106	0.0161
Axial 9	0.0239	0.0159	0.0190	0.0127	0.0238	0.0158	0.0193	0.0129	0.0335	0.0223	0.0385	0.0256	0.0291	0.0199	0.0294	0.0197	0.0292	0.0196	0.0244	0.0162	0.0196	0.0131	0.0297	0.0199
Dif	0.0091	0.0081	0.0074	0.0063	0.0092	0.0082	0.0071	0.0060	0.0129	0.0115	0.0149	0.0130	0.0113	0.0095	0.0111	0.0097	0.0115	0.0099	0.0101	0.0083	0.0081	0.0069	0.0123	0.0107
R	0.3816	0.5080	0.3919	0.4993	0.3883	0.5166	0.3667	0.4633	0.3837	0.5150	0.3861	0.5061	0.3893	0.4770	0.3785	0.4903	0.3926	0.5066	0.4115	0.5147	0.4104	0.5229	0.4149	0.5393
S	0.0168	0.0296	0.0192	0.0292	0.0171	0.0307	0.0182	0.0350	0.0136	0.0241	0.0128	0.0238	0.0145	0.0270	0.0132	0.0281	0.0144	0.0259	0.0148	0.0268	0.0190	0.0328	0.0176	0.0276